Dear Topical Editor,

Dear Executive Editor,

Thank you for your helpful comments on the revised version of our manuscript. Admittedly, the two points that you mention can be addressed in a better way:

Editor *Reviewer 2 requests an explanation of the main features of a karst system, to provide a better context for the model equations:*

> *"Referee #2 The reader is rather rushed into the main part of the paper, and detailed comments are provided below on the introduction. However, it is strongly suggested that to provide a proper context for the equations in Section 2.1 then a basic explanation of the main features of a karst system is provided."*

No such explanation was added, and the changes to Section 2 largely consist of moving a section of text from Section 2.1, which is insufficient to address this major reviewer comment. Please add a suitable description of the system such that the reader understands the choice of model formulation.

Our response We agree with the Editor that such a description would improve readability. Therefore in the second revised version of the manuscript we expanded subsection 2.1 by a description of the surface and shallow subsurface processes that are typical for karst regions:

> "The structure of the VarKarst-R model (Figure 1a) is based on the conceptual understanding of the surface and shallow subsurface processes of karst regions (Figure 1c). Their most characteristic feature is the existence of the epikarst that evolves close to the surface because of stronger carbonate rock dissolution. It can be seen as a temporal storage and distribution system for karst recharge (Aquilina et al., 2006; Williams, 1983a). Depending on the rates of infiltration, variability of soil thicknesses and hydraulic conductivities, it can produce slow and diffuse vertical percolation into the carbonate rock, or it can concentrate infiltration laterally towards dissolution widened fissures or conduits (Hartmann et al., 2012). Applied on a 0.25 x 0.25 decimal degree grid (Figure 1b), VarKarst-R simulates potential recharge, whichdecimal degree grid (Figure 1b), VarKarst-R simulates potential recharge, which …"

Editor *Reviewer 1 also comments on the same section:*

> *"Referee #1 Section 2.1 is a brief summary of equations previously published by the Author and appears to be shown here for the purpose of explaining the four parameters. This could be stated more clearly because it's not totally clear whether these are new equations or not. Also, the reader would need to read the previous papers to fully understand their meaning. One reason for the confusion is that this is described as being a new version (VarKarst-R), but the equations have not changed (unless I missed something). Therefore, please explain what was modified in the new version."*

This comment has not yet been sufficiently addressed. If I am correct in guessing that the model equations (1-9) are copied from a previous paper, please state that explicitly at the top of the section

and provide the reference. The referee comment that it is not possible to fully understand their meaning from the current paper has also not been addressed. I found it very difficult to understand the description of these equations, for example in Equation 2, it is unclear whether these three equations are assumptions, definitions or derivations, or how they follow from each other. It is unclear why an integral rather than a sum is taken over a discrete number of model compartments. It is unclear what 'left' and 'right' refer to (line 130), and what is the link with Figure 1.

Our response We clarified the differences between model features that are adopted from previous studies and the new aspects of the study at the very beginning of Section 2, where we inserted the following text:

> "…is estimated by a modified version of the VarKarst model (Hartmann et al., 2013a, 2014c). The model has shown to be applicable at various scales and climates over Europe (Hartmann et al., 2013b). To simulate karst recharge we discard the groundwater routines originally present in VarKarst but we use exactly the same surface and shallow subsurface routines. The resulting recharge simulation model, VarKarst-R, is described in the next subsection. The main novel feature of the large-scale application of the VarKarst-R model is the estimation of its parameters. While previous applications of the VarKarst model could rely on calibration by observations at the karst system outlet, the simulation of large-scale recharge requires a different approach. We developed a new parameter estimation procedure of VarKarst-R that separates the study area into four karst landscapes by cluster analysis and estimates model parameters and their uncertainty by a step-wise parameter confinement process (explained in subsection 2.3)"

Furthermore, more information was added throughout Subsection 2.1, clarifying what was taken from previous studies and what is the role of different equations in relation to the description of the karst recharge processes that were also newly added (see above). In particular, the confusing part of Equation (2) was removed and an elaboration of its purpose and a reference to the original paper was added instead:

> "For the application of a priori information of mean soil storage capacities (subsection 2.3) $V_{max,S}$ has to be derived from the mean soil storage capacity V_{soil} by (Hartmann et al., 2013b):
>
> $$V_{\max,S} = V_{soil} \cdot 2^{\left(\frac{a}{a+1}\right)}. \quad (1)$$
>
> Preceding work (Hartmann et al., 2013a) showed …"

Please find below a version of the re-revised manuscript with all changes marked.

We hope that our second set of revisions improved the manuscript to a level that is acceptable to be published in Geoscientific Model Development.

Kind regards,

Andreas Hartmann

A large-scale simulation model to assess karstic groundwater recharge over Europe and the Mediterranean

A. Hartmann[1,3], Tom Gleeson[2], Rafael Rosolem[1], Francesca Pianosi[1], Yoshihide Wada[4], Thorsten Wagener[1]

[1] Department of Civil Engineering, University of Bristol, United Kingdom

[2] Civil Engineering, McGill University, Canada

[3] Faculty of Environment and Natural Resources, University of Freiburg, Germany

[4] Department of Physical Geography, Utrecht University, The Netherlands

Correspondence to: A. Hartmann (aj.hartmann@bristol.ac.uk)

Re-resubmitted to Geoscientific Model Development May 2015

Abstract

Karst develops through the dissolution of carbonate rock and is a major source of groundwater contributing up to half of the total drinking water supply in some European countries. Previous approaches to model future water availability in Europe are either too-small scale or do not incorporate karst processes, i.e. preferential flow paths. This study presents the first simulations of groundwater recharge in all karst regions in Europe with a parsimonious karst hydrology model. A novel parameter confinement strategy combines *a priori* information with recharge-related observations (actual evapotranspiration and soil moisture) at locations across Europe while explicitly identifying uncertainty in the model parameters. Europe's karst regions are divided into 4 typical karst landscapes (humid, mountain, Mediterranean and desert) by cluster analysis and recharge is simulated from 2002 to 2012 for each karst landscape. Mean annual recharge ranges from negligible in deserts to

>1 m/a in humid regions. The majority of recharge rates ranges from 20%-50% of precipitation and are sensitive to sub-annual climate variability. Simulation results are consistent with independent observations of mean annual recharge and significantly better than other global hydrology models that do not consider karst processes (PCR-GLOBWB, WaterGAP). Global hydrology models systematically underestimate karst recharge implying that they over-estimate actual evapotranspiration and surface runoff. Karst water budgets and thus information to support management decisions regarding drinking water supply and flood risk are significantly improved by our model.

1 Introduction

Groundwater is the main source of water supply for billions of people in the world (Gleeson et al., 2012). Carbonate rock regions only constitute about 35% of Europe's land surface (Williams and Ford, 2006), yet contribute up to 50% of the national water supply in some European countries (COST, 1995) because of their high storage capacity and permeability (Ford and Williams, 2007). Climate conditions have a primary control on groundwater recharge (de Vries and Simmers, 2002). Climate simulations suggest that in the next 90 years Mediterranean regions will be exposed to higher temperatures and lower precipitation amounts (Christensen et al., 2007). In addition, shifts in hydrological regimes (Milly et al., 2005) and hydrological extremes (Dai, 2012; Hirabayashi et al., 2013) can be expected. To assess the impact of climate change on regional groundwater resources as groundwater depletion or deteriorations of water quality, large-scale simulation models are necessary that go beyond the typical scale of aquifer simulation models (~10-10,000 km²) Additionally, we expect the future variability of climate to be beyond that reflected in historical observations, which means that model predictions should derive credibility via more in-depth diagnostic evaluation of the consistency between the model and the underlying system and not from some calibration exercise (Wagener et al., 2010).

Currently available global hydrology models discretise the land surface in grids with a resolution down to 0.25 to 0.5 decimal degrees. Parts of the vertical fluxes are well represented, e.g. the energy balance (Ek, 2003; Miralles et al., 2011). But groundwater recharge and groundwater flow are represented simply by heuristic equations (Döll and Fiedler, 2008a) or assumptions of linearity (Wada et al., 2010, 2014). They do not explicitly simulate a dynamic water table or regional groundwater flow. Global models also assume

61 homogenous conditions of hydrologic and hydraulic properties in each of their grid cells,
62 rather than variable flow paths, and they completely omit the possibility of preferential flow.
63 This was criticized in the recent scientific discourse about the need for large-scale hyper-
64 resolution models (Beven and Cloke, 2012; Wood et al., 2011).

65 The assumption of homogeneity is certainly inappropriate for karst regions. Chemical
66 weathering of carbonate rock and other physical processes develop preferential pathways and
67 strong subsurface heterogeneity (Bakalowicz, 2005). Flow and storage are heterogeneous
68 ranging from very slow diffusion to rapid concentrated flow at the surface, in the soil, the
69 unsaturated zone and the aquifer (Kiraly, 1998). A range of modeling studies have developed
70 and applied karst specific models at individual karst systems at the catchment or aquifer scale
71 (Doummar et al., 2012; Fleury et al., 2007; Hartmann et al., 2013b; Le Moine et al., 2008) but
72 a lack of *a priori* information of aquifer properties and observations of groundwater dynamics
73 have prohibited their application on larger scales (Hartmann et al., 2014a).

74 Compared to the limited information about the deeper subsurface there is much better
75 information about the surface and shallow subsurface including maps of soil types and
76 properties (FAO/IIASA/ISRIC/ISSCAS/JRCv, 2012), observations of soil moisture
77 (International Soil Moisture Network, Dorigo et al., 2011) and of latent heat fluxes (FluxNet,
78 Baldocchi et al., 2001), as well as river discharge (GRDC, 2004). Surface and shallow
79 subsurface information is used for the parameterization and evaluation of the surface routines
80 of present large-scale models. But, although these data also cover Europe's karst regions, it
81 has not been used for the development of large-scale models to simulate karstic surface and
82 shallow subsurface flow and storage dynamics.

83 The objective of this study is to develop the first large-scale simulation model for karstic
84 groundwater recharge over Europe and the Mediterranean. Despite much broader definitions
85 of groundwater recharge (e.g., Lerner et al., 1990), we focus on potential recharge, that is
86 vertical percolation from the soil below the depth affected by evapotranspiration. We use a
87 novel type of model structure that considers the sub-grid heterogeneity of karst properties
88 using statistical distribution functions. To achieve a realistic parameterization of the model we
89 identify typical karst landscapes by cluster analysis and by a combined use of *a priori*
90 information about soil storage capacities and observations of recharge related fluxes and
91 storage dynamics. Applying a parameter confinement strategy based on Monte Carlo

sampling we are able to provide large-scale simulation of annual recharge including a quantification of their uncertainty.

2 Data and Methods

Due to chemical weathering (karstification) karst systems have a strong subsurface heterogeneity of flow and storage processes (Bakalowicz, 2005) that have to be considered to produce realistic simulations (Hartmann et al., 2014a). In this study, large-scale karst recharge is estimated by a modified version of the VarKarst model (Hartmann et al., 2013a, 2014c). The model has shown to be applicable at various scales and climates over Europe (Hartmann et al., 2013b). To simulate karst recharge we discard the groundwater routines originally present in VarKarst but we use exactly the same surface and shallow subsurface routines. The resulting recharge simulation model, VarKarst-R, is described in the next subsection. The main novel feature of the large-scale application of the VarKarst-R model is the estimation of its parameters. While previous applications of the VarKarst model could rely on calibration by observations at the karst system outlet, the simulation of large-scale recharge requires a different approach. We developed a new parameter estimation procedure of VarKarst-R that separates the study area into four karst landscapes by cluster analysis and estimates model parameters and their uncertainty by a step-wise parameter confinement process (explained in subsection 2.3).

2.1 The model

The structure of the VarKarst-R model (Figure 1~~Figure 1~~a) is based on the conceptual understanding of the surface and shallow subsurface processes of karst regions (Figure 1~~Figure 1~~c). Their most characteristic feature is the existence of the epikarst that evolves close to the surface because of stronger carbonate rock dissolution. It can be seen as a temporal storage and distribution system for karst recharge (Aquilina et al., 2006; Williams, 1983a). Depending on the rates of infiltration, variability of soil thicknesses and hydraulic conductivities, it can produce slow and diffuse vertical percolation into the carbonate rock, or it can concentrate infiltration laterally towards dissolution widened fissures or conduits (Hartmann et al., 2012). Applied on a 0.25 x 0.25 decimal degree grid (Figure 1~~Figure 1~~b), VarKarst-R simulates potential recharge, which is the water column that~~e~~ vertically percolate~~sd~~ from the soil and epikarst. Hence, the previous version of the model (VarKarst) is reduced to include only the soil and the epikarst simulation routines but still using the same

statistical distribution functions that allow for variable soil depths, variable epikarst depths and variable subsurface dynamics (Figure 1~~Figure 1~~). This leads to a parametrically efficient process representation. Comparisons with independently derived field data showed that these distribution functions are a good approximation of the natural heterogeneity (Hartmann et al., 2014b).

In VarKarst and VarKarst-R, heterogeneity of soil depths is represented by a mean soil storage capacity V_{soil} [mm] and a variability constant a [-]. The soil storage capacity $V_{S,i}$ [mm] for every compartment i is defined by:

$$V_{S,i} = V_{\max,S} \cdot \left(\frac{i}{N}\right)^a \quad (1)$$

where $V_{max,S}$ [mm] is the maximum soil storage capacity and N is the total number of model compartments. For the application of a priori information of mean soil storage capacities (subsection 2.3), $V_{max,S}$~~This is~~ has to be derived from the mean soil storage capacity V_{soil} ~~as~~by (Hartmann et al., 2013b):

$$V_{\max,S} = V_{soil} \cdot 2^{\left(\frac{a}{a+1}\right)}. \quad (2)$$

~~where $i_{1/2}$ is the compartment at which the soil storage capacities on the left equal the soil storage capacities on the right (Figure 1a).~~ Preceding work (Hartmann et al., 2013a) showed that the same distribution coefficient a can be used to derive the epikarst storage distribution $V_{E,i}$ from the mean epikarst storage capacity V_{epi} [mm] (via the maximum epikarst storage $V_{max,E}$ likewise to $V_{max,S}$ in Eq (2)):

$$V_{E,i} = V_{\max,E} \cdot \left(\frac{i}{N}\right)^a \quad (3)$$

At each time step t, the actual evapotranspiration from each soil compartment $E_{act,i}$ is ~~found~~ derived by reducing potential evaporation according the soil moisture deficit:

$$E_{act,i}(t) = E_{pot}(t) \cdot \frac{\min\left[V_{Soil,i}(t) + P_{eff}(t) + Q_{Surface,i}(t), V_{S,i}\right]}{V_{S,i}} \quad (4)$$

where E_{pot} [mm] is the potential evapotranspiration derived by the Priestley-Taylor equation (Priestley and Taylor, 1972), P_{eff} [mm] is the sum of liquid precipitation and snow melt, $Q_{surface,i}$ [mm] is the surface inflow arriving from compartment i-1 (see Eq. (9)), and $V_{S,i}$ [mm]

the water stored in the soil at time step *t*. Snow fall and snow melt are derived from daily snow water equivalent available from GLDAS-2 (Table 1~~Table 1~~). During days with snow cover we set $E_{act}(t)$=0. Flow from the soil to the epikarst $R_{Epi,i}$ [mm] takes place when the soil storages are fully saturated. It is calculated by:

Formatiert: Englisch (USA)

$$R_{Epi,i}(t) = \max\left[V_{Soil,i}(t) + P_{eff}(t) + Q_{Surface,i}(t) - E_{act,i}(t) - V_{S,i}, 0\right] \quad (5)$$

The temporal water storage of the epikarst is drained ~~F~~following an assumption of linearity (Rimmer and Hartmann, 2012), which is controlled by the epikarst storage coefficients $K_{E,i}$ [d] ~~controls the epikarst outflow dynamics~~:

$$Q_{Epi,i}(t) = \frac{\min\left[V_{Epi,i}(t) + R_{Epi,i}(t), V_{E,i}\right]}{K_{E,i}} \cdot \Delta t \quad (6)$$

$$K_{E,i} = K_{Epi} \cdot \left(\frac{N - i + 1}{N}\right)^{a} \quad (7)$$

where $V_{E,i}$ [mm] is the water stored in compartment *i* of the epikarst at time step *t*. Again, the same distribution coefficient *a* is applied to derive $K_{E,i}$ from the mean epikarst storage coefficient K_{Epi}. The latter is obtained from the mean epikarst storage coefficient K_{epi} using (Hartmann et al., 2013b):

$$K_{\max,E} = K_{epi} \cdot (a + 1) \quad (8)$$

When infiltration exceeds the soil and epikarst storage capacities, lateral flow concentration initiates. S~~s~~urface flow to the next model compartment $Q_{Surf,i+1}$ [mm] ~~initiates~~is calculated by~~:~~

$$Q_{Surf,i+1}(t) = \max\left[V_{Epi,i}(t) + R_{Epi,i}(t) - V_{E,i}, 0\right] \quad (9)$$

Depending on the volumes of excess water surface flow can be produced at several model compartments resulting in significant amounts of laterally concentrated percolation where it finally infiltrates (Figure 1a). To summarize, the model is completely defined by the four parameters *a*, K_{epi}, V_{soil}, and V_{epi} (Table 2~~Table 2~~).

2.2 Data availability

Forcing for the VarKarst-R model is derived through the Global Land Data Assimilation System (GLDAS-2) that assimilates satellite- and ground-based observational data products to obtain optimal fields of land surface states and fluxes (Rodell et al., 2004; Rui and Beaudoing,

2013). While precipitation, temperature and net radiation are mainly merged from satellite and gauge observations, snow water equivalent is derived using data assimilation as well as the snow water equivalent simulations of the NOAH land surface model v3.3 (Ek, 2003) driven by GLDAS-2 forcing. Europe's and the Mediterranean's carbonate rock areas are derived from a global map (vector data) of carbonate rock (Williams and Ford, 2006). Each cell of the 0.25 decimal degree simulation grid intersecting a carbonate rock region was considered a karst region. The model was calibrated and evaluated with observations of actual evapotranspiration from the FLUXNET (Baldocchi et al., 2001) and with soil water content data from the International Soil Moisture Network ISMN (Dorigo et al., 2011). Only stations within carbonate rock regions and with ≥12 months of available data were used (Figure 2~~Figure 2~~). Months with <25 days of observations were discarded. In addition, months with ≥50% mismatch in their energy closure were discard from the FLUXNET data set (similar to Miralles et al., 2011).

2.3 Parameter estimation

A lack of *a priori* information and observations of discharge and groundwater levels that can be used for calibration are the primary reasons why karst models have not been applied on larger scales yet (Hartmann et al., 2014a). The parameter assessment strategy we present in the following is meant to overcome this problem by using a combination of *a priori* information and recharge-related variables. We define typical karst landscapes over Europe and the Mediterranean and apply this combined information to a large initial sample of possible model parameter sets. In a step-wise process we then discard all parameter sets that produce simulations inconsistent with our *a priori* information and our recharge-related observations.

2.3.1 Definition of typical karst landscapes

Our definition of typical karst landscapes is based on the well-known the hydrologic landscape concept (Winter, 2001), which describes hydrological landscapes based on their geology, relief and climate. Constraining ourselves to karst regions that mainly develop on carbonate rock we assume that differences among the karst landscapes are due to differences in relief and climate, and the consequent processes of landscape evolution including the weathering of carbonate rock (karstification). The carbonate rock regions in Europe and the Mediterranean are divided into typical landscapes using simple descriptors of relief (range of

altitude RA) and climate (aridity index AI and mean annual number of days with snow cover DS) within each of 0.25 decimal degree grid cells and a standard cluster analysis scheme (k-means method). We test the quality of clustering for 2 to 20 clusters by calculating the sums of squared internal distances to the cluster means. The so-called "elbow method" identifies the point where adding additional clusters only leads to a marginal reduction in the internal distance metric, i.e. the percentage of variance explained by adding more clusters would not increase significantly (Seber, 2009).

2.3.2 Model parameters for each karst landscape

We initially sample 25,000 possible model parameter sets from independent uniform distributions using parameter ranges derived from previous catchment scale applications of the VarKarst-R model over Europe and the Mediterranean (Table 2~~Table 2~~). We use *a priori* information and recharge-related observations to assess parameter performance for each karst landscape. *A priori* information consists of spatially distributed information about mean soil storage capacities as provided by several preceding mapping and modelling studies (Ek, 2003; FAO/IIASA/ISRIC/ISSCAS/JRCv, 2012; Miralles et al., 2011). Recharge-related variables are (1) soil moisture observations and (2) observations of actual evaporation at various locations over the modelling domain (Table 1~~Table 1~~, Figure 2~~Figure 2~~). Soil moisture is related to recharge because it indicates the start and duration of saturation of the soil during which diffuse and preferential recharge can take place. Actual evaporation is related to recharge because usually no surface runoff occurs in karst regions due to the high infiltration capacities (Jeannin and Grasso, 1997). The difference of monthly precipitation and actual evaporation is therefore a valid proxy for groundwater recharge at a monthly time scale or above. The new parameter confinement strategy is applied to each of the karst landscapes in 3 steps:

1. Bias rule: retain only the parameter sets that produce a bias between observed and simulated actual evaporation lower than 75% at all FLUXNET locations within the chosen karst landscape:

$$\min_i\left(bias_i\right)=\min_i\left(\frac{\mu_{sim,i}-\mu_{obs,i}}{\mu_{obs,i}}\right)\overset{!}{<}75\% \qquad (10)$$

Where $m_{sim,i}$ and $m_{obs,i}$ are the sum of simulated and observed actual evapotranspiration at location i, respectively. The value 75% was found by trial-and-error, which reduced

the initial sample to a reasonable number. The bias rule was not applied on the soil moisture since porosities of the soil matrix were not available prohibiting a comparison of simulated and observed soil water contents.

2. Correlation rule: retain only the parameter sets that produce a positive coefficient of (Pearson) correlation between observations and simulations of both actual evaporation and soil moisture, at all locations:

$$\left(\min_i \left[corr(AET_{sim,i}, AET_{obs,i} \right] \wedge \min_j \left[corr(\theta_{sim,j}, \theta_{obs,j} \right] \right) \overset{!}{>} 0 \qquad (11)$$

where $AET_{sim,j}$ and $AET_{obs,j}$, and $\theta_{sim,j}$ and $\theta_{obs,j}$ are the monthly means of simulated and observed actual evapotranspiration, and soil water content at locations *i/j*, respectively.

3. Application of *a priori* information: retain only parameter sets in which V_{soil} falls within the feasible ranges that can be derived from *a priori* information about the maximum soil storage capacity in different karst landscapes (Ek, 2003; FAO/IIASA/ISRIC/ISSCAS/JRCv, 2012; Miralles et al., 2011). Less than usual we add the *a priori* information at the last step to evaluate if the *posterior* distributions of V_{soil} already adapt to the ranges defined in this confinement step. If they do not we would conclude that the recharge related information applied in confinement steps 1 and 2 is biased. If they do, we have indication that the data applied in all 3 steps is complementary.

Each step reduces the initial parameter sample differently for each of the karst landscapes. The *posterior* parameter distributions within the confined samples should be different among the karst landscapes if the karst landscapes are properly defined. The rather weak thresholds in step 1 and 2 were chosen to take into account the uncertainties resulting from the differences in scales of observations (point) and simulations (grid cell), and from the indirect observation of recharge (actual evaporation and soil moisture as recharge related variables).

2.4 Recharge simulations over Europe and the Mediterranean

Recharge is simulated over the carbonate regions of Europe and the Mediterranean from 2002/03 to 2011/12 using the confined parameter samples for each of the identified karst landscapes and the available forcings (Table 1~~Table 1~~). The mean and standard deviation of

simulated recharge for each grid cell and time step is calculated by uniform discrete sampling of a representative subset of 250 parameter sets from each of the confined parameters sets which we regarded to be large enough to provide a reliable measure of spread.

2.5 Model evaluation

To assess the realism of simulated groundwater recharge we compare simulated with observed mean annual recharge volumes derived independently from karst studies over Europe and the Mediterranean (Table 3~~Table 3~~). In addition, we compare our results to the simulated mean annual recharge volumes of two well-established global simulation models: PCR-GLOBWB (Wada et al., 2010, 2014) and WaterGAP (Döll and Fiedler, 2008a; Döll et al., 2003).

We furthermore apply a global sensitivity analysis strategy, called Regional Sensitivity Analysis (Spear and Hornberger, 1980), to evaluate the importance of the 4 model parameters at different simulation time scales ranging from 1 month up to 10 years. This analysis shows (1) which simulated process and characteristics are dominant at a given time scale and (2) which parameters will need more careful calibration when the model will be used in future studies. We use the same sample of 25,000 parameter sets that was created for the parameter estimation strategy (subsection 2.3.2) and assess the sensitivity of 4 model outputs representative of different time scales: coefficient of variation (CV) of simulated monthly recharge volumes (monthly), CV of simulated 3-monthly recharge volumes (seasonal), CV of annual recharge volumes (annual), and total recharge over the entire 10-year simulation period (decadal). We do not consider temporal resolution less than a month given the assumption that the difference of precipitation and actual evapotranspiration can be a proxy for groundwater recharge, and due to uncertainties related to differences in simulation (grid cell) and observation (point).

For each of the identified karst landscapes we choose the 10 locations that are closest to their cluster means (Euclidean distances to relief and climate descriptors; subsection 2.3.1) as representative locations. In the regional sensitivity analysis approach, we split the parameter sets into two groups, those that produce simulations above the simulated median of one of the 4 model outputs and those that produce simulations below. We then calculate the maximum distance D(x) between marginal cumulative distribution functions (CDFs) produced by these

two distributions for each of the parameters – a large distance D(x) suggests that the parameter is important for simulating this particular output (Figure 3~~Figure 3~~).

3 Results

3.1 Parameter assessment

3.1.1 Definition of typical karst landscapes

Cluster analysis resulted in four clusters, which are generally spatially contiguous (Figure 4~~Figure 4~~) and have quantitatively distinct cluster means (Table 4~~Table 4~~). We can attribute particular characteristics to each cluster using the mean values of the clustering descriptors (Table 4~~Table 4~~): (1) Humid hills and plains (HUM) are characterised by an aridity index <1, a significant number of days with snow cover and low elevation differences. (2) High range mountains (MTN) have an aridity index of ~1, they also have a significant number of days with snow cover and they show very large topographic elevation differences. (3) Mediterranean medium range mountains (MED) show a high aridity index, only few days with snow cover and high elevation differences. (4) Desert hills and plains (DES) are described by similar altitude ranges as the humid hills and plains but they have a high aridity indices and almost no days with snow cover. The karst landscapes order from North (HUM) to South (DES) based on increasing temperatures and decreasing precipitation amounts. While HUM and DES appear to be separated clearly, MTN and MED mix in some regions, for instance Greece and Turkey where mountainous regions are in close proximity to the coast.

3.1.2 Model parameter estimates for each karst landscape

The three steps of the new parameter confinement strategy resulted in a significant reduction of the initial sample of 25,000 parameter sets (Figure 5~~Figure 5~~). Each step has a different impact on the reduction among the identified landscapes. For the humid karst landscapes, the correlation rule appears to have the strongest impact while for the mountain and Mediterranean landscapes the bias rule results in the strongest reduction. For the desert landscape only step 3, i.e. application of *a priori* information, reduces the initial sample because no data was available to apply steps 1 and 2. Considering the parameter ranges for each landscape after the application of the confinement strategy (Table 5~~Table 5~~), we only

achieved a confinement of the distribution parameter a, the soil storage capacity V_{soil}, and slight confinement of the epikarst storage coefficient K_{epi}.

The impact of the three confinement steps becomes more obvious when considering their *posterior* distributions (Figure 6~~Figure 6~~). The distributions of parameters a, K_{epi} and V_{soil} evolve significantly away from their initial uniform distributions along the confinement steps. In general, changes of the *posterior* distributions of each landscape's parameter samples are in accordance with the reductions of their number (Figure 5~~Figure 5~~), though changes are pronounced differently among the parameters. While a and V_{soil} change strongly for HUM, MTN and MED, V_{epi} maintains a uniform distribution across all steps. K_{epi} also exhibits strong changes for HUM but they are less pronounced for MTN and MED. The *posterior* distributions of the DES landscape do not change except for step 3 due to the lack of information to apply confinement steps 1 and 2. Step 3 results in a tailoring of the distribution of V_{soil} for all landscapes. For HUM, MTN and MED it can be seen that confinement steps 1 and 2 already pushed the parameter distributions towards their final shape, meaning that the changes in parameter distributions induced by the comparison with observations are consistent with the *a priori* information about the physical characteristics of the karst.

3.2 Recharge simulations over Europe and the Mediterranean

The parameter confinement strategy allows us to apply VarKarst-R over all of Europe and the Mediterranean, and to obtain recharge simulations for the hydrological years 2002/03-2011/12. Thanks to the 250 parameter sets that we samples from the *posterior* parameter distributions we can include an estimate of uncertainty for each grid cell (Figure 7~~Figure 7~~). Mean annual recharge ranges from almost 0 to >1000 mm/a with the highest volumes found in Northern UK, the Alps and former Yugoslavia. The lowest values are found in the desert regions of Northern Africa. The vast majority of recharge rates ranges from 20%-50% of precipitation. Considering the simulations individually for each karst landscape reveals that the mountain landscapes produce the largest recharge volumes followed by the humid and Mediterranean landscapes (Figure 8~~Figure 8~~a). The desert landscapes produce the lowest recharge volumes. However, the recharge rates reveal that on average the Mediterranean landscapes show the largest recharge rates, followed by the highly variable mountains (Figure 8~~Figure 8~~c). Humid and deserts landscapes exhibit lower recharge rates. Uncertainties, expressed by the standard deviation of the 250 simulations for each grid cell, are rather low, seldom exceeding 35 mm/a (Figure 8~~Figure 8~~b). However, expressed as coefficients of

variation, most of them range from 5%-25% for the humid, mountain and Mediterranean landscapes but for the desert landscape they can reach up to 50% of the mean annual recharge (Figure 8~~Figure 8~~d).

3.3 Model evaluation

We compare the simulated recharge volumes of our model with recharge volumes assessed from independent and published karst studies over Europe and the Mediterranean (Figure 9~~Figure 9~~a). Even though there is a considerable spread across the simulations their bulk plots well around the 1:1 line achieving an average deviation of only -58 mm/a (Table 6~~Table 6~~). Considering the individual karst landscapes there is an over-estimation of recharge for the humid landscapes and an under-estimation for the mountain landscapes. The best results are achieved for the Mediterranean landscapes with only slight under-estimation (Figure 9~~Figure 9~~a). When we compare the same observations to the simulated recharge volumes of the PCR-GLOBWB (Figure 9~~Figure 9~~b) and WaterGAP models (Figure 9~~Figure 9~~c) we find a strong tendency of under-estimation that is strongest for the mountain and Mediterranean landscapes but still significant for the humid landscapes (Table 6~~Table 6~~). For the humid landscapes absolute deviations are similar for PCR-GLOBWB and VarKarst-R.

In addition to comparing simulated and observed annual averages, sensitivity analysis on the model output gives us insight in the realism of the model and the importance of individual model parameters at different time scales (Figure 10~~Figure 10~~). Our results show that parameters a and V_{soil} have the overall strongest influence on the simulated recharge from a monthly to a 10-year time scale but their influence decreases toward shorter time scales. Simultaneously the epikarst parameter K_{epi} gains more importance. This behaviour is most pronounced for the Mediterranean and desert landscapes. The same is true for V_{epi}, but its overall importance remains much lower, which was also found in the parameter confinement strategy (Figure 6~~Figure 6~~).

4 Discussion

4.1 Reliability of parameter estimation

4.1.1 Identification of karst landscapes

The identification of different karst landscapes is a crucial step within our new parameter estimation strategy. The four karst landscapes we identified depend mostly on the choice of climatic and topographic descriptors (Table 4~~Table 4~~) and the selected number of clusters. Even though neglecting several factors as depositional environments, fracturing by tectonic processes or regional variations in rain acidity our choice of descriptors is well justified from our understanding of dominant hydrologic process controls as formalized in the hydrologic landscape concept (Winter, 2001) and applied similarly at many other studies (Leibowitz et al., 2014; Sawicz et al., 2011; Wigington et al., 2013). The appropriate choice of clusters for the k-means method is less unambiguous (Ketchen and Shook, 1996). The change in number of clusters when the sum of squared distances to our cluster centres only reduces marginally was not clearly definable (Figure A 1~~Figure A 1~~). However, choosing only 3 clusters instead of 4 would have resulted in unrealistic spatial distribution of clusters. The attribution of Northern African regions with Northern Europe to the same cluster occurred because of their similarity of altitude ranges (Table 4~~Table 4~~). On the other hand, a selection of 5 clusters would have resulted in a cluster with properties just between the MTN and the MED clusters and, because of a much stronger scattering, weaker spatial distinction between them. With 4 clusters our karst landscapes are similar to the Koeppen Geiger climate regions (Kottek et al., 2006), in particular the Oceanic Climate (HUM), the Hot and Warm summer Mediterranean Climate (MED), and the Hot Desert Climates (DES). We see deviations when comparing the Polar and Alpine Climate regions of Koeppen-Geiger with our High Range Mountain karst landscape though, since our landscapes are also defined by their elevation ranges.

The borders of these hydrologic landscapes are also uncertain. Natural systems usually do not have straight borders that fall on a grid as assumed by this analysis. Typical transitions between landscape types are continuous and hence transitions from a parameter set representing one landscape to another parameter set of another cluster should be graded, as well. This will be discussed in the following subsection.

4.1.2 Confinement of parameters

How the 3 steps of the parameter confinement strategy reduce the initial sample shows which type of data provides the most relevant information for each of the karst landscapes. While the timing of actual evapotranspiration and soil saturation that is expressed by the correlation rule appears to be most relevant for the humid landscapes, the bias rule, which represents the volumes of monthly evapotranspiration is more relevant for the mountain and Mediterranean landscapes. Swapping the order of the correlation rule and the bias rule would provide the same results for HUM and MTN. But for MED the alternative order increases the importance of timing expressed by the correlation rule indicating the similar importance of both confinement steps.

The thresholds we set in confinement step 1 and 2 are not very strict, and the ranges of soil storage capacity we used as *a priori* information in step 3 are quite large This compensates for the fact that (1) only recharge-related variables are available rather than direct recharge observations, (2) these variables are not available at the simulation scale (0.25° grid) but at a point-scale, and (3) the transition between the landscapes is more continuous than discrete. Despite these rather weak constraints, the initial parameter sample of 25,000 reduces to a quite low numbers between 679 (HUM) and 2,731 (MED). All *posterior* parameters overlap except for the soil storage capacities that are tailored by the *a priori* information (confinement step 3). Hence, a little number of parameter sets for one landscape is also acceptable for some of the other landscape and therefore taking into account the continuous transition between them.

All model parameters, except for V_{epi}, show different shapes in their cumulative distribution functions across the karst landscapes. The desert landscape parameters only differ from the initial sample for the V_{soil} parameter due to the lack of information to apply confinement steps 1 and 2. The distribution parameter *a* is found at the lower values of its feasible range for the humid and mountain landscapes indicating a significant contribution of preferential recharge. Since altitude ranges are rather low for HUM this may be attributed to a significant epikarst development (Perrin et al., 2003; Williams, 1983b). For MTN a mixture of epikarst development and topography driven interflow at the mountain hill slopes and valleys can be expected to control the dynamics of karstic recharge (Scanlon et al., 2002; Tague and Grant, 2009). At the Mediterranean landscapes the *a* parameter adapts to ranges that are rather found at the higher values of its initial range indicating that there is a stronger differentiation

between diffuse and concentrated recharge. This may be due to the generally thinner soils (Table 5~~Table 5~~) that limit the availability of CO_2 for karst evolution (Ford and Williams, 2007). Instead, local surface runoff channels the water to the next enlarged fissure or crack to reach the subsurface as concentrated recharge (Lange et al., 2003). The epikarst storage coefficient K_{epi} for HUM and MED is at lower values of the initial range indicating realistic mean residence times of days to weeks (Aquilina et al., 2006; Hartmann et al., 2013a). The MTN landscapes show larger K_{epi} values indicating slower epikarst dynamics most probably due to the reasons mentioned above. The application of *a priori* information in confinement step 3 automatically tailors the values of V_{soil} to ranges that we assume to be realistic. The fact that confinement steps 1 and 2 already push the shape of their *posteriors* towards the *a priori* ranges corroborates that assumption.

The little changes that occur to the initial distributions of the DES parameter sets elaborate the flexibility of our parameter assessment strategy. The *posterior* distribution evolves only where information is available (for this landscape on V_{soil}). This is also evident in the behaviour of parameter V_{epi}. The available information is just not precise enough to achieve identification beyond its *a priori* ranges. For parameter *a* in HUM, MTN and MED, a lot of information is derived from the available data and its *posteriors* differ strongly from its initial distribution, while there is less information to determine K_{epi}. This explicit handling of uncertainties in the parameter identification process allows us to provide recharge simulations over Europe's karst regions with uncertainty estimates that represent confidence for each of the identified karst landscapes.

4.2 Simulation of karst recharge over Europe and the Mediterranean

4.2.1 Realism of spatial patterns

Simulated mean annual recharge amounts for the period 2002/03-2011/12 show a wide range of values, from 0 >1000 mm/a (Figure 7~~Figure 7~~). Total water availability (mean annual precipitation) appears to be the main driver for its spatial pattern in many regions, for instance at former Yugoslavia or Northern UK. This is consistent with findings of other studies (Hartmann et al., 2014c; Samuels et al., 2010). When we normalize the recharge rates by the observed precipitation amounts we find that water availability is not the only control on mean annual recharge volumes. A strong relation of evapotranspiration and karst characteristics and processes was shown in many studies and is also found here (Heilman et al., 2014; Jukic and

Denic-Jukic, 2008). Potential evaporation is generally increasing from North to South and has an important impact on recharge rates as well; for instance on the Arabian Peninsula or in the Alps.

Mountain ranges are considered to be the water towers of the world (Viviroli et al., 2007). Here the MTN landscapes also show the largest recharge volumes due to the large precipitation volumes they receive, though with a considerable spread in our study. HUM and MED landscapes behave similarly with significantly less recharge than MTN. Not surprisingly there is not much recharge in the desert landscapes at all. But the differences among the clusters shift when considering recharge rates. Due to their thin soils, and therefore low soil storage for evaporation (Table 5~~Table 5~~), the DES karst landscapes transfer up to 45% of the little precipitation they receive into recharge. The MED landscapes show similarly high recharge rates. Though since their soils are generally thicker than the DES soils the typical seasonal and convective rainfall patterns of the Mediterranean climate (Goldreich, 2003; Lionello, 2012) might have an important impact, too.

Even though there is still considerable spread in our confined parameter sets, the uncertainty in simulated mean annual recharge volumes is quite low. The uncertainties that follow the limited information contained in the observations are revealed more clearly when we relate the standard deviation of simulated recharge to its mean volumes with the coefficient of variation. The uncertainty for the DES landscape is the largest among the clusters because *a priori* information is only available for V_{soil}. The uncertainty reduces for the MED and MTN landscapes. The low uncertainties for the coefficient of variation of our recharge simulations for the HUM landscape indicate that the available data contained significant information for confining the model parameter ranges.

4.2.2 Relevance of different recharge processes to simulation time scales

The mean annual water balance of a hydrological system is dominated by the separation of precipitation into actual evapotranspiration and discharge (Budyko and Miller, 1974; Sivapalan et al., 2011). Actual evapotranspiration is controlled by the soil storage capacity V_{soil} and the distribution coefficient a within the VarKarst-R model. Regional sensitivity analysis shows that both of them are most sensitive for the 10-year and annual time scale (Figure 10~~Figure 10~~). Both parameters loose some impact at higher temporal resolutions (seasonal or monthly time scale) in favour of the parameters that control the dynamics of the epikarst. This behaviour is consistent with evidence from field and other modelling studies

that showed that the epikarst can be considered as a temporary storage and distribution system for karstic recharge (Hartmann et al., 2012; Williams, 1983b) – potentially storing water for several days to weeks (Aquilina et al., 2006; Hartmann et al., 2013a). Parameter V_{epi} does not show much sensitivity across all landscapes as suggested by the *posterior* distributions of the confinement strategy. First of all, this finding indicates that the data we used for our confinement strategy do not bias the general model behaviour. It also shows that for the epikarst storage and flow dynamics K_{epi} is much more important when simulating at monthly or seasonal resolution.

Furthermore, the results of the regional sensitivity analysis show which parameters are most important at a given time scale. Depending on the purpose a new study may start with the initial ranges of the model parameters or it might continue with the confined parameter ranges that we found here. The latter would result in slightly different sensitivities (Figure A 2~~Figure A 2~~). For both cases, the epikarst parameters will require more attention when applying the VarKarst-R model for simulations at seasonal or monthly time scales. When working at a smaller spatial scale, combined analysis of spring discharge and its hydrochemistry may provide such additional information (Lee and Krothe, 2001; Mudarra and Andreo, 2011). When working at a time scale of >1 year the variability constant a and the soil storage capacity V_{soil} require most attention if one starts from the initial ranges. The distribution parameter is most important when using the confined ranges. Again, spring discharge analysis may help to understand the degree of karstification (Kiraly, 2003) and the distribution of concentrated and diffuse recharge mechanisms that are controlled by a. In addition, more precise digital elevation models or soil maps may help to better identify a and V_{soil}. A limitation of the regional sensitivity analysis approach used here is that parameter interactions are only included implicitly, considering parameter interactions with more elaborate methods (Saltelli et al., 2008) may reveal even more characteristics of the VarKarst-R model at different simulation time scales. But this is beyond the scope of this paper.

4.3 Impact of karstic subsurface heterogeneity

Even though some deviations occur among the individual karst landscapes, the general simulations of the VarKarst-R model follow well the observations of mean annual recharge rates over Europe and the Mediterranean (Figure 9~~Figure 9~~). On the other hand, the widely-used large-scale simulation models PCR-GLOBWB (Wada et al., 2010, 2014) and WaterGAP (Döll and Fiedler, 2008b; Döll et al., 2003) generally under-estimate groundwater recharge

(Table 6~~Table 6~~). The reason for this is the representation of karstic subsurface heterogeneity within the VarKarst-R model, i.e. the inclusion of preferential flowpaths and of subsurface heterogeneity. Based on the conceptual understanding of soil and epikarst storage behaviour (Figure 1~~Figure 1~~c) it allows (1) for more recharge during wet conditions because surface runoff is not generated, and (2) for more recharge during dry conditions because the thin soil compartments will always allow for some water to percolate downwards before it is consumed by evapotranspiration. During wet conditions, both PCR-GLOBWB and WaterGAP would produce surface runoff instead that is subsequently lost from groundwater recharge. During dry conditions, due to its non-variable soil storage capacity, the PCR-GLOBWB model would not produce any recharge when the soil water is below its minimum storage. Separating surface runoff and groundwater recharge by a constant factor the WaterGAP model would produce recharge during dry conditions, but a constant fraction of effective precipitation will always become fast surface/subsurface runoff resulting in reduced recharge volumes.

This does not mean that the representation of recharge processes in models like PCR-GLOBWB or WaterGAP is generally wrong, but can be limited since our analysis shows that the structures of such models need more adaption to the particularities of different hydrologic landscapes. In particular it adds to the need for incorporating sub-grid heterogeneity in our large-scale simulation models (Beven and Cloke, 2012). Karst regions comprise about 35% of Europe's land surface and our results indicate that presently their groundwater recharge is under-estimated, while surface runoff and actual evaporation are over-estimated. Given the expected decrease of precipitation in semi-arid regions, such as the Mediterranean, and an increase of extreme rainfall events at the same time in the near future (2016-2035, Kirtman et al., 2013) current large-scale simulation models will over-estimate both the vulnerability of groundwater recharge and the flood hazard in karst regions in Europe and the Mediterranean. The same is true for the long-term future (end of 21st century, Collins et al., 2013). Of course, an over-estimation of vulnerability and hazard might be the "lesser evil" compared to an over-estimation. But at times of limited financial resources excessive investments in ensuring the security of drinking water supply and flood risk management for potential future changes may unnecessarily aggravate the socio-economic impacts of climate change.

Formatiert: Englisch (Großbritannien)

5 Conclusions

In this study we have presented the first attempt to model groundwater recharge over all karst regions in Europe and the Mediterranean. The model application was made possible by a novel parameter confinement strategy that utilized a combination of *a priori* information and recharge related observations on 4 typical karst landscapes that were identified through cluster analysis. Handling the remaining uncertainty explicitly as *posterior* parameter distributions resulting from the confinement strategy we were finally able to produce recharge simulations and an estimate of their uncertainty. We found an adequate agreement with our new model when comparing our results with independent observations of recharge at study sites over Europe and the Mediterranean. We further show that current large-scale modelling approaches tend to significantly under-estimate recharge volumes.

Overall, our analysis showed that the subsurface heterogeneity of karst regions and the presence of preferential flowpaths enhances recharge. It results in high infiltration capacities prohibiting surface runoff and reducing actual evapotranspiration during wet conditions. On the other hand it allows for recharge during dry conditions because some water can always percolate downwards passing the thin fraction of the distributed soil depths. This particular behaviour suggests that karstic regions might be more resilient to climate change in terms of both flooding and droughts. Drinking water and flood risk management is liable to be based on erroneous information at least at the 35% of Europe's land surface since this is not considered in current large-scale modelling approaches.

However, using recharge directly as a proxy for "available" groundwater resources may not be good in all cases, neither in karst regions nor in other types of aquifers (Bredehoeft, 2002). To precisely estimate the sustainably usable fraction of groundwater the aquifer outflow should be known rather than just the inflow. Further pumpingstrategies should consider the geometry and transmissivity of the aquifer. Hence, recharge estimation can be considered only as a first proxy of available groundwater and future studies should focus on the large-scale simulation of karst groundwater flow and storage to further improve water resources predictions in karst regions.

Acknowledgements

We want to thank Juergen Strub, research associate at the Chair of Hydrology, Freiburg, Germany, for designing some of the figures and Thomas Godman for collecting references to independent recharge studies. This work was supported by a fellowship within the Postdoc

Programme of the German Academic Exchange Service [Andreas Hartmann, DAAD] and by the UK Natural Environment Research Council [Francesca Pianosi, CREDIBLE Project; grant number NE/J017450/1]. The sensitivity analysis was carried out by the SAFE Toolbox (http://bristol.ac.uk/cabot/resources/safe-toolbox/). We thank Petra Döll for providing the mean annual recharge volumes of WaterGAP, and Fanny Sarazin for checking the results of the regional sensitivity analysis. The article processing charge was funded by the open access publication fund of the Albert Ludwigs University Freiburg.

References

Allocca, V., Manna, F. and De Vita, P.: Estimating annual groundwater recharge coefficient for karst aquifers of the southern Apennines (Italy), Hydrol. Earth Syst. Sci., 18(2), 803–817, doi:10.5194/hess-18-803-2014, 2014.

Andreo, B., Vías, J., Durán, J., Jiménez, P., López-Geta, J. and Carrasco, F.: Methodology for groundwater recharge assessment in carbonate aquifers: application to pilot sites in southern Spain, Hydrogeol. J., 16(5), 911–925 [online] Available from: http://dx.doi.org/10.1007/s10040-008-0274-5, 2008.

Aquilina, L., Ladouche, B. and Doerfliger, N.: Water storage and transfer in the epikarst of karstic systems during high flow periods, J. Hydrol., 327, 472–485, 2006.

Arnell, N. W.: Relative effects of multi-decadal climatic variability and changes in the mean and variability of climate due to global warming : future streamflows in Britain, J. Hydrol., 270, 195–213, 2003.

Aydin, H., Ekmekci, M. and Soylu, M. E.: Characterization and conceptualization of a relict karst aquifer (bilecik , turkey) karakterizacija in konceptualizacija reliktnega, Acta carsologica, 42(1), 75–92, 2013.

Bakalowicz, M.: Karst groundwater: a challenge for new resources, Hydrogeol. J., 13, 148–160, 2005.

Bakalowicz, M., El, Æ. M. and El-hajj, A.: Karst groundwater resources in the countries of eastern Mediterranean : the example of Lebanon, Environ. Geol., 54, 597–604, doi:10.1007/s00254-007-0854-z, 2008.

Baldocchi, D., Falge, E., Gu, L., Olson, R., Hollinger, D., Running, S., Anthoni, P., Bernhofer, C., Davis, K., Evans, R., Fuentes, J., Goldstein, A., Katul, G., Law, B., Lee, X., Malhi, Y., Meyers, T., Munger, W., Oechel, W., Paw, K. T., Pilegaard, K., Schmid, H. P., Valentini, R., Verma, S., Vesala, T., Wilson, K. and Wofsy, S.: FLUXNET: A New Tool to Study the Temporal and Spatial Variability of Ecosystem–Scale Carbon Dioxide, Water Vapor, and Energy Flux Densities, Bull. Am. Meteorol. Soc., 82(11), 2415–2434, doi:10.1175/1520-0477(2001)082<2415:fantts>2.3.co;2, 2001.

Formatiert: Englisch (Großbritannien)

635 Barbieri, M., Boschetti, T., Petitta, M. and Tallini, M.: Stable isotope (2H, 18O and
636 87Sr/86Sr) and hydrochemistry monitoring for groundwater hydrodynamics analysis in a
637 karst aquifer (Gran Sasso, Central Italy), Appl. Geochemistry, 20(11), 2063–2081,
638 doi:10.1016/j.apgeochem.2005.07.008, 2005.

639 Beven, K. J. and Cloke, H. L.: Comment on "Hyperresolution global land surface modeling:
640 Meeting a grand challenge for monitoring Earth's terrestrial water" by Eric F. Wood et al.,
641 Water Resour. Res., 48(1), W01801, doi:10.1029/2011WR010982, 2012.

642 Bonacci, O.: Analysis of the maximum discharge of karst springs, Hydrogeol. J., 9(4), 328–
643 338, doi:10.1007/s100400100142, 2001.

644 Bredehoeft, J. D.: The water budget myth revisited: why hydrogeologists model, Ground
645 Water, 40(4), 340–345, 2002.

646 Budyko, D. H. and Miller, M. I.: Climate and life, Academic press, New York., 1974.

647 Butscher, C. and Huggenberger, P.: Intrinsic vulnerability assessment in karst areas: A
648 numerical modeling approach, Water Resour. Res., 44, W03408,
649 doi:10.1029/2007WR006277, 2008.

650 Christensen, J. H., Hewitson, B., Busuioc, A., Chen, A., Gao, X., Held, I., Jones, R., Kolli, R.
651 K., Kwon, W.-T., Laprise, R., Rueda, V. M., Mearns, L., Menéndez, C. G., Räisänen, J.,
652 Rinke, A., Sarr, A. and Whetton, P.: Regional Climate Projections, in Climate Change 2007:
653 The Physical Science Basis. Contribution of Working Group I to the Fourth Assessment
654 Report of the Intergovernmental Panel on Climate Change, edited by S. Solomon, D. Qin, M.
655 Manning, Z. Chen, M. Marquis, K. B. Averyt, M. Tignor, and H. L. Miller, p. 996,
656 Cambridge University Press, Cambridge, United Kingdom and New York, NY, USA. [online]
657 Available from:
658 http://www.ipcc.ch/publications_and_data/publications_ipcc_fourth_assessment_report_wg1_
659 report_the_physical_science_basis.htm, 2007.

660 Collins, M., Knutti, R., Arblaster, J. M., Dufresne, J.-L., Fichefet, T., Friedlingstein, P., Gao,
661 X., Gutowski, W. J., Johns, T. and Krinner, G.: Long-term climate change: projections,
662 commitments and irreversibility, in Climate Change 2013: The Physical Science Basis.
663 Contribution of Working Group I to the Fifth Assessment Report of the Intergovernmental
664 Panel on Climate Change, edited by T. F. Stocker, D. Qin, G.-K. Plattner, M. Tignor, S. K.
665 Allen, J. Boschung, A. Nauels, Y. Xia, V. Bex, and P. M. Midgley, pp. 1029–1136,
666 Cambridge University Press, Cambridge, United Kingdom and New York, NY, USA., 2013.

667 COST: COST 65: Hydrogeological aspects of groundwater protection in karstic areas, Final
668 report (COST action 65), edited by D.-G. X. I. I. S. European Comission Research and
669 Development, Eur. Comm. Dir. XII Sci. Res. Dev., Report EUR, 446, 1995.

670 Dai, A.: Increasing drought under global warming in observations and models, Nat. Clim.
671 Chang., 3(1), 52–58, doi:10.1038/nclimate1633, 2012.

672 Döll, P. and Fiedler, K.: Global-scale modeling of groundwater recharge, Hydrol. Earth Syst.
673 Sci., 12(3), 863–885, doi:10.5194/hess-12-863-2008, 2008a.

674 Döll, P. and Fiedler, K.: Global-scale modeling of groundwater recharge, Hydrol. Earth Syst.
675 Sci., 12(3), 863–885, doi:10.5194/hess-12-863-2008, 2008b.

676 Döll, P., Kaspar, F. and Lehner, B.: A global hydrological model for deriving water
677 availability indicators: model tuning and validation, J. Hydrol., 270(1-2), 105–134,
678 doi:10.1016/S0022-1694(02)00283-4, 2003.

679 Dorigo, W. A., Wagner, W., Hohensinn, R., Hahn, S., Paulik, C., Xaver, A., Gruber, A.,
680 Drusch, M., Mecklenburg, S., van Oevelen, P., Robock, A. and Jackson, T.: The International
681 Soil Moisture Network: a data hosting facility for global in situ soil moisture measurements,
682 Hydrol. Earth Syst. Sci., 15(5), 1675–1698, doi:10.5194/hess-15-1675-2011, 2011.

683 Doummar, J., Sauter, M. and Geyer, T.: Simulation of flow processes in a large scale karst
684 system with an integrated catchment model (Mike She) – Identification of relevant parameters
685 influencing spring discharge, J. Hydrol., 426-427, 112–123,
686 doi:10.1016/j.jhydrol.2012.01.021, 2012.

687 Einsiedl, F.: Flow system dynamics and water storage of a fissured-porous karst aquifer
688 characterized by artificial and environmental tracers, J. Hydrol., 312, 312–321, 2005.

689 Ek, M. B.: Implementation of Noah land surface model advances in the National Centers for
690 Environmental Prediction operational mesoscale Eta model, J. Geophys. Res., 108(D22),
691 doi:10.1029/2002jd003296, 2003.

692 FAO/IIASA/ISRIC/ISSCAS/JRCv: Harmonized World Soil Database (version 1.2), edited by
693 FAO/IIASA, 2012.

694 Fleury, P., Plagnes, V. and Bakalowicz, M.: Modelling of the functioning of karst aquifers
695 with a reservoir model: Application to Fontaine de Vaucluse (South of France), J. Hydrol.,
696 345, 38–49, 2007.

697 Ford, D. C. and Williams, P. W.: Karst Hydrogeology and Geomorphology, Wiley,
698 Chichester., 2007.

699 Foster, S. S. D.: Groundwater recharge and pollution vulnerability of British aquifers: a
700 critical overview, Geol. Soc. London, Spec. Publ., 130, 7–22,
701 doi:10.1144/GSL.SP.1998.130.01.02, 1998.

702 Gleeson, T., Moosdorf, N., Hartmann, J. and van Beek, L. P. H.: A glimpse beneath earth's
703 surface: GLobal HYdrogeology MaPS (GLHYMPS) of permeability and porosity, Geophys.
704 Res. Lett., n/a–n/a, doi:10.1002/2014gl059856, 2014a.

705 Gleeson, T., Moosdorf, N., Hartmann, J. and van Beek, L. P. H.: A glimpse beneath earth's
706 surface: GLobal HYdrogeology MaPS (GLHYMPS) of permeability and porosity, Geophys.
707 Res. Lett., 41(11), 3891–3898, doi:10.1002/2014GL059856, 2014b.

708 Gleeson, T., Wada, Y., Bierkens, M. F. and van Beek, L. P.: Water balance of global aquifers
709 revealed by groundwater footprint, Nature, 488(7410), 197–200, doi:10.1038/nature11295,
710 2012.

Goldreich, Y.: The climate of Israel: observation, research and application, Kluwer Academic/Plenum Publishers., 2003.

GRDC: Long Term Mean Annual Freshwater Surface Water Fluxes into the World Oceans, Comparisons of GRDC freshwater flux estimate with literature. [online] Available from: http://grdc.bafg.de/servlet/is/7083/, 2004.

Hartmann, A., Barberá, J. A., Lange, J., Andreo, B. and Weiler, M.: Progress in the hydrologic simulation of time variant recharge areas of karst systems – Exemplified at a karst spring in Southern Spain, Adv. Water Resour., 54, 149–160, doi:10.1016/j.advwatres.2013.01.010, 2013a.

Hartmann, A., Goldscheider, N., Wagener, T., Lange, J. and Weiler, M.: Karst water resources in a changing world: Review of hydrological modeling approaches, Rev. Geophys., DOI: 10.1002/2013rg000443, doi:10.1002/2013rg000443, 2014a.

Hartmann, A., Kobler, J., Kralik, M., Dirnböck, T., Humer, F. and Weiler, M.: Transit time distributions to understand the biogeochemical impacts of storm Kyrill on an Austrian karst system, Biogeosciences, submitted, 2015.

Hartmann, A., Lange, J., Weiler, M., Arbel, Y. and Greenbaum, N.: A new approach to model the spatial and temporal variability of recharge to karst aquifers, Hydrol. Earth Syst. Sci., 16(7), 2219–2231, doi:10.5194/hess-16-2219-2012, 2012.

Hartmann, A., Mudarra, M., Andreo, B., Marin, A., Wagener, T. and Lange, J.: Modeling spatio-temporal impacts of hydro-climatic extremes on a karst aquifer in Southern Spain, Water Resour. Res., moderate revisions, resubmit until July 2014, doi:10.1002/2014WR015685, 2014b.

Hartmann, A., Mudarra, M., Andreo, B., Marín, A., Wagener, T. and Lange, J.: Modeling spatiotemporal impacts of hydroclimatic extremes on groundwater recharge at a Mediterranean karst aquifer, Water Resour. Res., n/a–n/a, doi:10.1002/2014WR015685, 2014c.

Hartmann, A., Weiler, M., Wagener, T., Lange, J., Kralik, M., Humer, F., Mizyed, N., Rimmer, A., Barberá, J. A., Andreo, B., Butscher, C. and Huggenberger, P.: Process-based karst modelling to relate hydrodynamic and hydrochemical characteristics to system properties, Hydrol. Earth Syst. Sci., 17(8), 3305–3321, doi:10.5194/hess-17-3305-2013, 2013b.

Hatipoglu-Bagci, Z. and Sazan, M. S.: Characteristics of karst springs in Aydıncık (Mersin , Turkey), based on recession curves and hydrochemical and isotopic parameters, Q. J. Eng. Geol. Hydrogeol., 47(1), 89–99, 2014.

Heilman, J. L., Litvak, M. E., McInnes, K. J., Kjelgaard, J. F., Kamps, R. H. and Schwinning, S.: Water-storage capacity controls energy partitioning and water use in karst ecosystems on the Edwards Plateau, Texas, Ecohydrology, 7(1), 127–138, doi:10.1002/eco.1327, 2014.

748 Hirabayashi, Y., Mahendran, R., Koirala, S., Konoshima, L., Yamazaki, D., Watanabe, S.,
749 Kim, H. and Kanae, S.: Global flood risk under climate change, Nat. Clim. Chang., 3(9), 816–
750 821, doi:10.1038/nclimate1911, 2013.

751 Hoetzl, H.: Groundwater recharge in an arid karst area (Saudi Arabia), IAHS Publ.
752 (International Assoc. Hydrol. Sci., 232, 195–207, 1995.

753 Hughes, A. G., Mansour, M. M. and Robins, N. S.: Evaluation of distributed recharge in an
754 upland semi-arid karst system: the West Bank Mountain Aquifer, Middle East, Hydrogeol. J.,
755 16, 845–854, 2008.

756 Jackson, C. R., Meister, R. and Prudhomme, C.: Modelling the effects of climate change and
757 its uncertainty on UK Chalk groundwater resources from an ensemble of global climate
758 model projections, J. Hydrol., In Press, doi:10.1016/j.jhydrol.2010.12.028, 2010.

759 Jeannin, P.-Y. and Grasso, D. A.: Permeability and hydrodynamic behavior of karstic
760 environment, in Karst Waters Environmental Impact, edited by G. Gunay and A. I. Johnson,
761 pp. 335–342, A.A. Balkema, Roterdam., 1997.

762 Jukic, D. and Denic-Jukic, V.: Estimating parameters of groundwater recharge model in
763 frequency domain: Karst springs Jadro and Žrnovnica, Hydrol. Process., 22, 4532–4542,
764 2008.

765 Ketchen, D. J. and Shook, C. L.: The application of cluster analysis, Strateg. Manag. J.,
766 17(November 1994), 441–458, 1996.

767 Kiraly, L.: Modelling karst aquifers by the combined discrete channel and continuum
768 approach, Bull. d'Hydrogéologie, 16, 77–98, 1998.

769 Kiraly, L.: Karstification and Groundwater Flow, Speleogenes. Evol. Karst Aquifers, 1(3), 1–
770 24, 2003.

771 Kirtman, B., Power, S. B., Adedoyin, J. A., Boer, G. J., Bojariu, R., Camilloni, I., Doblas-
772 Reyes, F. J., Fiore, A. M., Kimoto, M. and Meehl, G. A.: Near-term climate change:
773 projections and predictability, in Climate Change 2013: The Physical Science Basis.
774 Contribution of Working Group I to the Fifth Assessment Report of the Intergovernmental
775 Panel on Climate Change, edited by T. F. Stocker, D. Qin, G.-K. Plattner, M. Tignor, S. K.
776 Allen, J. Boschung, A. Nauels, Y. Xia, V. Bex, and P. M. Midgley, pp. 953–1028, Cambridge
777 University Press, Cambridge, United Kingdom and New York, NY, USA., 2013.

778 Kottek, M., Grieser, J., Beck, C., Rudolf, B. and Rubel, F.: World Map of the Köppen-Geiger
779 climate classification updated, Meteorol. Zeitschrift, 15(3), 259–263, doi:10.1127/0941-
780 2948/2006/0130, 2006.

781 Koutroulis, A. G., Tsanis, I. K., Daliakopoulos, I. N. and Jacob, D.: Impact of climate change
782 on water resources status: A case study for Crete Island, Greece, J. Hydrol., 479, 146–158,
783 doi:10.1016/j.jhydrol.2012.11.055, 2013.

Formatiert: Englisch (Großbritannien)

784 Lange, J., Greenbaum, N., Husary, S., Ghanem, M., Leibundgut, C. and Schick, A. P.: Runoff
785 generation from successive simulated rainfalls on a rocky, semi-arid, Mediterranean hillslope,
786 Hydrol. Process., 17(2), 279–296, doi:10.1002/hyp.1124, 2003.

787 Lee, E. S. and Krothe, N. C.: A four-component mixing model for water in a karst terrain in
788 south-central Indiana, USA. Using solute concentration and stable isotopes as tracers, Chem.
789 Geol., 179, 2001.

790 Leibowitz, S. G., Comeleo, R. L., Wigington Jr., P. J., Weaver, C. P., Morefield, P. E.,
791 Sproles, E. a. and Ebersole, J. L.: Hydrologic landscape classification evaluates streamflow
792 vulnerability to climate change in Oregon, USA, Hydrol. Earth Syst. Sci., 18(9), 3367–3392,
793 doi:10.5194/hess-18-3367-2014, 2014.

794 Lerner, D. N., Issar, A. S. and Simmers, I.: Groundwater recharge : a guide to understanding
795 and estimating natural recharge, Heise, Hannover., 1990.

796 Lionello, P.: The Climate of the Mediterranean Region: From the past to the future, Elsevier.,
797 2012.

798 Maloszewski, P., Stichler, W., Zuber, A. and Rank, D.: Identifying the flow systems in a
799 karstic-fissured-porous aquifer, the Schneealpe, Austria, by modelling of environmental 18O
800 and 3H isotopes, J. Hydrol., 256, 48–59, 2002.

801 Milly, P. C. D., Dunne, K. A. and Vecchia, A. V: Global pattern of trends in streamflow and
802 water availability in a changing climate, Nature, 438(7066), 347–350,
803 doi:10.1038/nature04312, 2005.

804 Miralles, D. G., Holmes, T. R. H., De Jeu, R. A. M., Gash, J. H., Meesters, A. G. C. A. and
805 Dolman, A. J.: Global land-surface evaporation estimated from satellite-based observations,
806 Hydrol. Earth Syst. Sci., 15(2), 453–469, doi:10.5194/hess-15-453-2011, 2011.

807 Le Moine, N., Andréassian, V. and Mathevet, T.: Confronting surface- and groundwater
808 balances on the La Rochefoucauld-Touvre karstic system (Charente, France), Water Resour.
809 Res., 44, W03403, doi:10.1029/2007WR005984, 2008.

810 Le Moine, N., Andréassian, V., Perrin, C. and Michel, C.: How can rainfall-runoff models
811 handle intercatchment groundwater flows? Theoretical study based on 1040 French
812 catchments, Water Resour. Res., 43, W06428, doi:10.1029/2006WR005608, 2007.

813 Mudarra, M. and Andreo, B.: Relative importance of the saturated and the unsaturated zones
814 in the hydrogeological functioning of karst aquifers: The case of Alta Cadena (Southern
815 Spain), J. Hydrol., 397(3-4), 263–280, doi:10.1016/j.jhydrol.2010.12.005, 2011.

816 Padilla, A., Pulido-Bosch, A. and Mangin, A.: Relative Importance of Baseflow and
817 Quickflow from Hydrographs of Karst Spring, Ground Water, 32(2), 267–277, 1994.

818 Perrin, J., Jeannin, P.-Y. and Zwahlen, F.: Epikarst storage in a karst aquifer: a conceptual
819 model based on isotopic data, Milandre test site, Switzerland, J. Hydrol., 279, 106–124, 2003.

820 Priestley, C. H. B. and Taylor, R. J.: On the Assessment of Surface Heat Flux and
821 Evaporation Using Large-Scale Parameters, Mon. Weather Rev., 100(2), 81–92,
822 doi:10.1175/1520-0493(1972)100<0081:OTAOSH>2.3.CO;2, 1972.

823 Quinn, J. J., Tomasko, D. and Kuiper, J. A.: Modeling complex flow in a karst aquifer,
824 Sediment. Geol., 184, 343–352, 2006.

825 Rimmer, A. and Hartmann, A.: Simplified conceptual structures and analytical solutions for
826 groundwater discharge using reservoir equations, Water Resour. Manag. Model. Ed. by DPC
827 Nayak, InTech, Kakinada, India, 217–338, 2012.

828 Rodell, M., Houser, P. R., Jambor, U., Gottschalck, J., Mitchell, K., Meng, C.-J., Arsenault,
829 K., Cosgrove, B., Radakovich, J., Bosilovich, M., Entin, J. K., Walker, J. P., Lohmann, D. and
830 Toll, D.: The Global Land Data Assimilation System, Bull. Am. Meteorol. Soc., 85(3), 381–
831 394, doi:10.1175/BAMS-85-3-381, 2004.

832 Rui, H. and Beaudoing, H.: README Document for Global Land Data Assimilation System
833 Version 2 (GLDAS-2) Products, GES DISC / HSL [online] Available from:
834 http://hydro1.sci.gsfc.nasa.gov/data/s4pa/GLDAS/README.GLDAS2.pdf, 2013.

835 Saltelli, A., Ratto, M., Andres, T., Campolongo, F., Cariboni, J., Gatelli, D., Saisana, M. and
836 Tarantola, S.: Global sensitivity analysis: the primer, John Wiley & Sons., 2008.

837 Samuels, R., Rimmer, A., Hartmann, A., Krichak, S. and Alpert, P.: Climate Change Impacts
838 on Jordan River Flow: Downscaling Application from a Regional Climate Model, J.
839 Hydrometeorol., 11(4), 860–879, doi:DOI 10.1175/2010JHM1177.1, 2010.

840 Sawicz, K., Wagener, T., Sivapalan, M., Troch, P. A. and Carrillo, G.: Catchment
841 classification: empirical analysis of hydrologic similarity based on catchment function in the
842 eastern USA, Hydrol. Earth Syst. Sci., 15(9), 2895–2911, doi:10.5194/hess-15-2895-2011,
843 2011.

844 Scanlon, B., Healy, R. and Cook, P.: Choosing appropriate techniques for quantifying
845 groundwater recharge, Hydrogeol. J., 10(1), 18–39 [online] Available from:
846 http://dx.doi.org/10.1007/s10040-001-0176-2, 2002.

847 Seber, G. A. F.: Multivariate observations, John Wiley & Sons., 2009.

848 Sivapalan, M., Yaeger, M. a., Harman, C. J., Xu, X. and Troch, P. a.: Functional model of
849 water balance variability at the catchment scale: 1. Evidence of hydrologic similarity and
850 space-time symmetry, Water Resour. Res., 47(2), W02522, doi:10.1029/2010WR009568,
851 2011.

852 Spear, R. C. and Hornberger, G. M.: Eutriphication in peel inlet - II. Identification of critical
853 uncertainties via generalized sensitivity analysis, Water Resour. Res., 14, 43–49, 1980.

854 Tague, C. and Grant, G. E.: Groundwater dynamics mediate low-flow response to global
855 warming in snow-dominated alpine regions, Water Resour. Res., 45(7), W07421,
856 doi:10.1029/2008WR007179, 2009.

Formatiert: Englisch (Großbritannien)

Formatiert: Englisch (Großbritannien)

857 Tritz, S., Guinot, V. and Jourde, H.: Modelling the behaviour of a karst system catchment
858 using non-linear hysteretic conceptual model, J. Hydrol., 397(3-4), 250–262,
859 doi:10.1016/j.jhydrol.2010.12.001, 2011.

860 USGS: Shuttle Radar Topography Mission, 3 Arc Second scene SRTM V2.1, edited by U. of
861 M. Global Land Cover Facility, 2006.

862 Vaute, L., Drogue, C., Garrelly, L. and Ghelfenstein, M.: Relations between the structure of
863 storage and the transport of chemical compounds in karstic aquifers, J. Hydrol., 199, 221–
864 238, 1997.

865 Vita, P. De, Allocca, V., Manna, F. and Fabbrocino, S.: Coupled decadal variability of the
866 North Atlantic Oscillation , regional rainfall and karst spring discharges in the Campania
867 region (southern Italy), , 1389–1399, doi:10.5194/hess-16-1389-2012, 2012.

868 Viviroli, D., Dürr, H. H., Messerli, B., Meybeck, M. and Weingartner, R.: Mountains of the
869 world, water towers for humanity: Typology, mapping, and global significance, Water
870 Resour. Res., 43(7), W07447, doi:10.1029/2006WR005653, 2007.

871 De Vries, J. J. and Simmers, I.: Groundwater recharge: an overview of processes and
872 challenges, Hydrogeol. J., 10(1), 5–17, doi:10.1007/s10040-001-0171-7, 2002.

873 Wada, Y., van Beek, L. P. H., van Kempen, C. M., Reckman, J. W. T. M., Vasak, S. and
874 Bierkens, M. F. P.: Global depletion of groundwater resources, Geophys. Res. Lett., 37(20),
875 L20402, doi:10.1029/2010gl044571, 2010.

876 Wada, Y., Wisser, D. and Bierkens, M. F. P.: Global modeling of withdrawal, allocation and
877 consumptive use of surface water and groundwater resources, Earth Syst. Dyn., 5(1), 15–40,
878 doi:10.5194/esd-5-15-2014, 2014.

879 Wagener, T., Sivapalan, M., Troch, P. A., McGlynn, B. L., Harman, C. J., Gupta, H. V,
880 Kumar, P., Rao, P. S. C., Basu, N. B. and Wilson, J. S.: The future of hydrology: An evolving
881 science for a changing world, Water Resour. Res., 46(5), W05301,
882 doi:10.1029/2009wr008906, 2010.

883 Wellings, S. R.: Recharge of the Upper Chalk aquifer at a site in Hampshire, England, J.
884 Hydrol., 69, 275–285, doi:10.1016/0022-1694(84)90167-7, 1984.

885 Wigington, P. J., Leibowitz, S. G., Comeleo, R. L. and Ebersole, J. L.: OREGON
886 HYDROLOGIC LANDSCAPES : A CLASSIFICATION FRAMEWORK 1, J. Am. Water
887 Resour. Assoc., 49(1), 163–182, doi:10.1111/jawr.12009, 2013.

888 Williams, P. W.: Journal of Hydrology, 61 (1983) 45--67, , 61, 45–67, 1983a.

889 Williams, P. W.: The role of the Subcutaneous zone in karst hydrology, J. Hydrol., 61, 45–67,
890 1983b.

891 Williams, P. W. and Ford, D. C.: Global distribution of carbonate rocks, Zeitschrift für
892 Geomorphol., Suppl. 147, 1–2, 2006.

Formatiert: Englisch (Großbritannien)

Winter, T. C.: The Concept of Hydrologic Landscapes, JAWRA J. Am. Water Resour. Assoc., 37(2), 335–349, doi:10.1111/j.1752-1688.2001.tb00973.x, 2001.

Wood, E. F., Roundy, J. K., Troy, T. J., van Beek, L. P. H., Bierkens, M. F. P., Blyth, E., de Roo, A., Döll, P., Ek, M., Famiglietti, J., Gochis, D., van de Giesen, N., Houser, P., Jaffé, P. R., Kollet, S., Lehner, B., Lettenmaier, D. P., Peters-Lidard, C., Sivapalan, M., Sheffield, J., Wade, A. and Whitehead, P.: Hyperresolution global land surface modeling: Meeting a grand challenge for monitoring Earth's terrestrial water, Water Resour. Res., 47(5), W05301, doi:10.1029/2010WR010090, 2011.

Zagana, E., Tserolas, P., Floros, G., Katsanou, K. and Andreo, B.: First outcomes from groundwater recharge estimation in evaporate aquifer in Greece with the use of APLIS method, in Advances in the Research of Aquatic Environment, edited by N. Lambrakis, G. Stournaras, and K. Katsanou, pp. 89–96, Springer Berlin Heidelberg., 2011.

Formatiert: Englisch (Großbritannien)

Formatiert: Englisch (Großbritannien)

907 ## Tables

908 **Table 1: Data availability, data properties and sources**

Variable	Spatial resolution	Time period	Frequency	Source	Reference
Precipitation	0.25°	2002-2012	daily	GLDAS-2	(Rodell et al., 2004; Rui and Beaudoing, 2013)
Temperature	0.25°	2002-2012	daily	GLDAS-2	
Net radiation	0.25°	2002-2012	daily	GLDAS-2	
Snow water equivalent	0.25°	2002-2012	daily	NOAHv3.3 /GLDAS-2	(Ek, 2003; Rodell et al., 2004)
Carbonate rock areas	vector data	-	-		(Williams and Ford, 2006)
Elevation	3''	-	-	SRMT V2.1	(USGS, 2006)
Rock permeability	vector data	-	-		(Gleeson et al., 2014a)
Actual evaporation	individual locations	individual periods	daily	FLUXNET	(Baldocchi et al., 2001)
Soil moisture	Individual locations	individual periods	daily	ISMN	(Dorigo et al., 2011)

909

910 **Table 2: Parameter description and initial ranges for Monte Carlo sampling based on previous field**
911 **studies and large-scale model applications**

Parameter	Unit	Description	Lower Limit*	Upper limit*	References
a	[-]	Variability constant	0	6	(Hartmann et al., 2013b, 2014c, 2015)
V_{soil}	[mm]	Mean soil storage capacity	0	1250	(Miralles et al., 2011; FAO/IIASA/ISRIC/ISSCAS/JRCv, 2012; Ek, 2003)
V_{epi}	[mm]	Mean epikarst storage capacity	200	700	(Perrin et al., 2003; Williams, 2008)
K_{epi}	[d]	Mean epikarst storage coefficient	0	50	(Gleeson et al., 2014b; Hartmann et al., 2013b)

912

913

914

915 **Table 3: Independent observations of mean annual recharge from field and modelling studies over Europe**
916 **and the Mediterranean**

Location	Latitude	Longitude	Mean annual recharge	Method	Author
(country, province)	[dec. degr.]	[dec. degr.]	[mm]		
Austria (Siebenquellen spring, Schneeaple)	47.69	15.6	694	observed water balance	(Maloszewski et al., 2002)
Croatia (Jadro spring, Dugopolje)	43.58	16.6	795	simulated water balance	(Jukic and Denic-Jukic, 2008)
Croatia (St. Ivan, Mirna)	45.22	13.6	386	observed water balance	(Bonacci, 2001)
France (Bonnieure, La Rouchefoucald-Touvre)	45.8	0.44	250	simulated water balance	(Le Moine et al., 2007)
France (Durzon spring, La Cavalerie)	44.01	3.16	378	observed water balance	(Tritz et al., 2011)
France (Fontaine de Vaucluse)	43.92	5.13	568	observed water balance	(Fleury et al., 2007)
France (St Hippolyte-du-Fort, Vidourle)	43.93	3.85	287	observed water balance	(Vaute et al., 1997)
Germany (Bohming spring, Rieshofen)	48.93	11.3	130	observed water balance	(Einsiedl, 2005)
Germany (Gallusquelle spring, Swabian Albs)	48.21	9.15	351	observed water balance	(Doummar et al., 2012)
Germany (Hohenfells)	49.2	11.8	200	observed water balance	(Quinn et al., 2006)
Greece (Arvi, Crete)*	35.13	24.55	241	observed water balance	(Koutroulis et al., 2013)
Greece (Aitoloakarnania)	38.60	21.15	484	empiric estimation method	(Zagana et al., 2011)
Italy (Cerella spring, Latina)	41.88	12.9	416	empiric estimation method	(Allocca et al., 2014)
Italy (Forcella spring, Sapri)	41.05	14.55	559	empiric estimation method	(Allocca et al., 2014)
Italy (Gran Sasso, Teramo)	42.27	13.34	700	observed water balance	(Barbieri et al., 2005)
Italy (Sanità)	40.78	15.13	974	observed water balance	(Vita et al., 2012)
Italy (Taburno spring)	39.9	15.81	693	empiric estimation method	(Allocca et al., 2014)
Lebanon (Anjar-Chamsine)	33.73	35.93	278	observed water balance	(Bakalowicz et al., 2008)
Lebanon (Zarka)	34.08	36.30	205	observed water balance	(Bakalowicz et al., 2008)
Lebanon (Afka)	34.05	35.95	842	observed water balance	(Bakalowicz et al., 2008)
Palestine (Mountain Aquifer)	~32.00	~35.30	144	simulated water balance	(Hughes et al., 2008)
Portugal (Algarve, minimum value)	~37.10	~-7.90	130	not mentioned	(de Vries and Simmers, 2002)
Portugal (Algarve, maximum value)	~37.10	~-7.90	300	not mentioned	(de Vries and Simmers, 2002)
Saudi Arabia (Eastern Arabian peninsula)	~26.50	~46.50	44	natural tracers	(Hoetzl, 1995)
Spain (Cazorla, Sierra de Cazorla)	37.9	-3.03	244	empiric estimation method	(Andreo et al., 2008)
Spain (La Villa spring, El Torcel)	36.93	-4.52	463	observed water balance	(Padilla et al., 1994)
Spain (Sierra de las Cabras, Arcos de la frontera)	36.65	-5.72	318	empiric estimation method	(Andreo et al., 2008)
Switzerland (Rappenfluh Spring)	47.87	7.67	650	simulated water balance	(Butscher and Huggenberger, 2008)
Turkey (Aydincik, Mersin)	36.97	33.22	552	observed water balance	(Hatipoglu-Bagci and Sazan, 2014)
Turkey (Harmankoy, Beyyayla)	40.15	30.65	32	observed water balance	(Aydin et al., 2013)
UK (Marlborough and Berkshire Downs and South-West Chilterns,	51.53	-1.15	146	simulated water balance	(Jackson et al., 2010)

minimum value)					
UK (Marlborough and Berkshire Downs and South-West Chilterns, maximum value)	51.53	-1.15	365	simulated water balance	(Jackson et al., 2010)
UK (Dorset)	50.75	-2.45	700	observed water balance	(Foster, 1998)
UK (Norfolk)	52.60	0.88	260	observed water balance	(Foster, 1998)
UK (Greta spring, Durham)	54.52	-1.87	690	observed water balance	(Arnell, 2003)
UK(R. Teme, Tenbury wells)	52.3	-2.58	355	observed water balance	(Arnell, 2003)
UK(Lambourn)	51.5	-1.53	234	observed water balance	(Arnell, 2003)
UK (Hampshire)	51.1	-1.26	348	observed water balance	(Wellings, 1984)

Table 4: Cluster means of the 4 identified karst landscapes (AI: aridity index, DS mean annual number of days with snow cover, RA: range of altitudes)

descriptor	unit	number of cluster/karst landscape			
		1.HUM	2.MTN	3.MED	4.DES
AI	[-]	0.80	0.98	3.18	20.00
DS	[a-1]	85	76	16	1
RA	[m]	228	1785	691	232

Table 5: Minima and maxima of the confined parameter samples for each of the identified landscapes

Parameter	Unit	HUM		MTN		MED		DES	
		min	max	min	max	min	max	min	max
a	[-]	1.1	3.3	0.3	2.9	0.8	6.0	0.1	6.0
V_{soil}*	[mm]	900.1 (900)	1248.9 (1250)	500.4 (500)	899.9 (900)	51.7 (50)	498.4 (500)	0.2 (0)	49.1 (500)
V_{epi}	[mm]	204.3	694.8	201.6	699.4	200.1	696.7	202.3	695.7
K_{epi}	[d]	0.0	35.8	7.3	49.9	0.0	48.4	10.4	49.9

* in brackets: *a priori* infromation used for step 3 of the parameter confinement strategy

Table 6: Mean deviations of the VarKarst-R, the PCR-GLOBWB model and the WaterGAP model from all observations and the individual regions

region	mean deviation [mm/a]		
	VarKarst-R	PCR-GLOBWB	WaterGAP
all	-58.3	-230.4	-264.2
HUM	65.5	-90.2	-151.6
MTN	-202.8	-427.5	-446.4
MED	-4.3	-217.3	-211.4

Figures

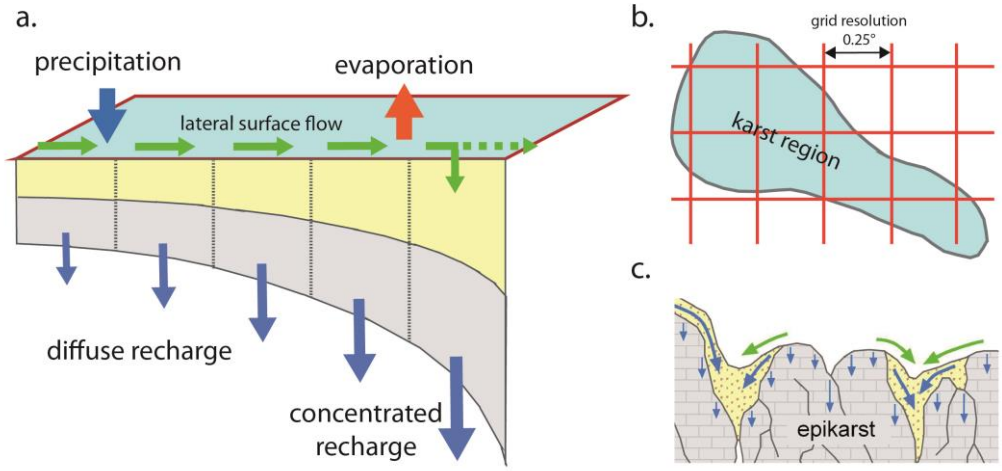

Figure 1: (a) schematic description of the model for one grid cell including the soil (yellow) and epikarst storages (grey) and the simulated fluxes, (b) its gridded discretisation over karst regions and (c) the subsurface heterogeneity that its structure represents for each grid cell.

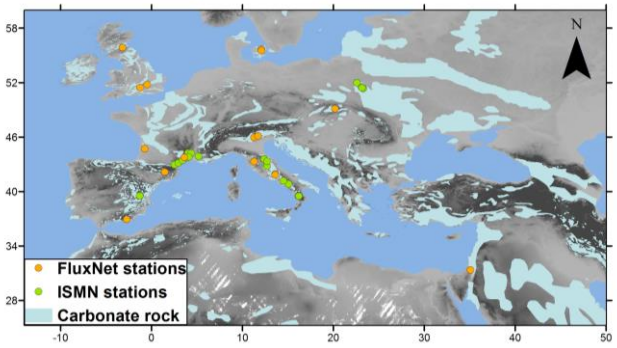

Figure 2: Carbonate rock areas over Europe and the Mediterranean, and location of the selected FLUXNET and ISMN stations

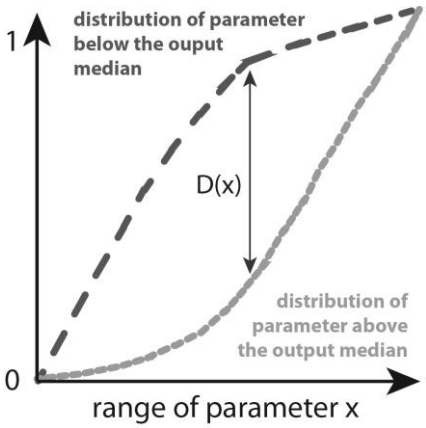

940

941 **Figure 3: Schematic elaboration of the regional sensitivity analysis procedure**

942

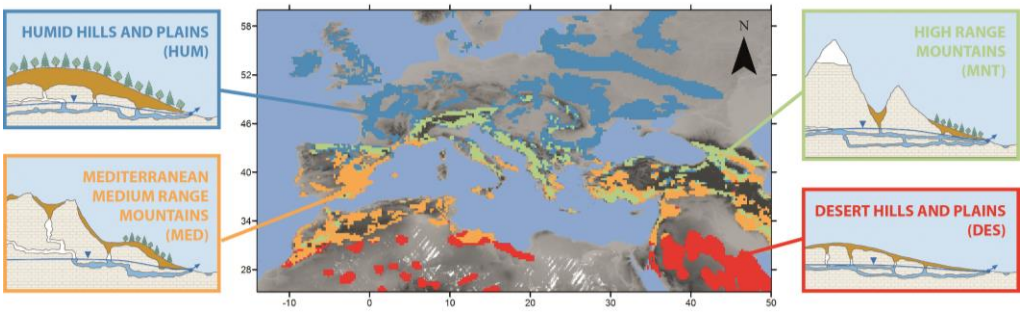

943

944 **Figure 4: Map with clusters and typical karst landscapes that were attributed to them**

945

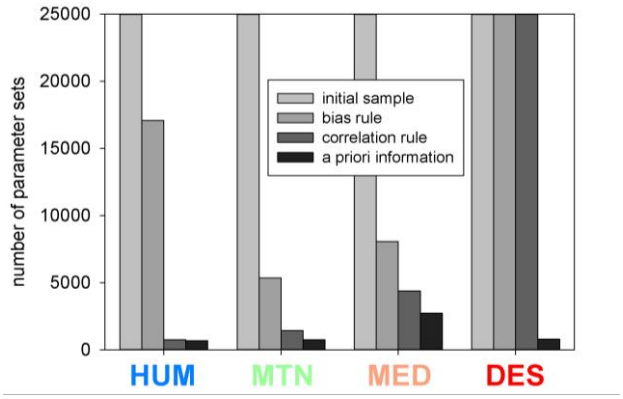

946

947 **Figure 5: Evolution of the initial sample of 25,000 parameter sets (each including the 4 model parameters**
948 **sampled from within their initial ranges) along the different confinement steps for the 4 karst landscapes**

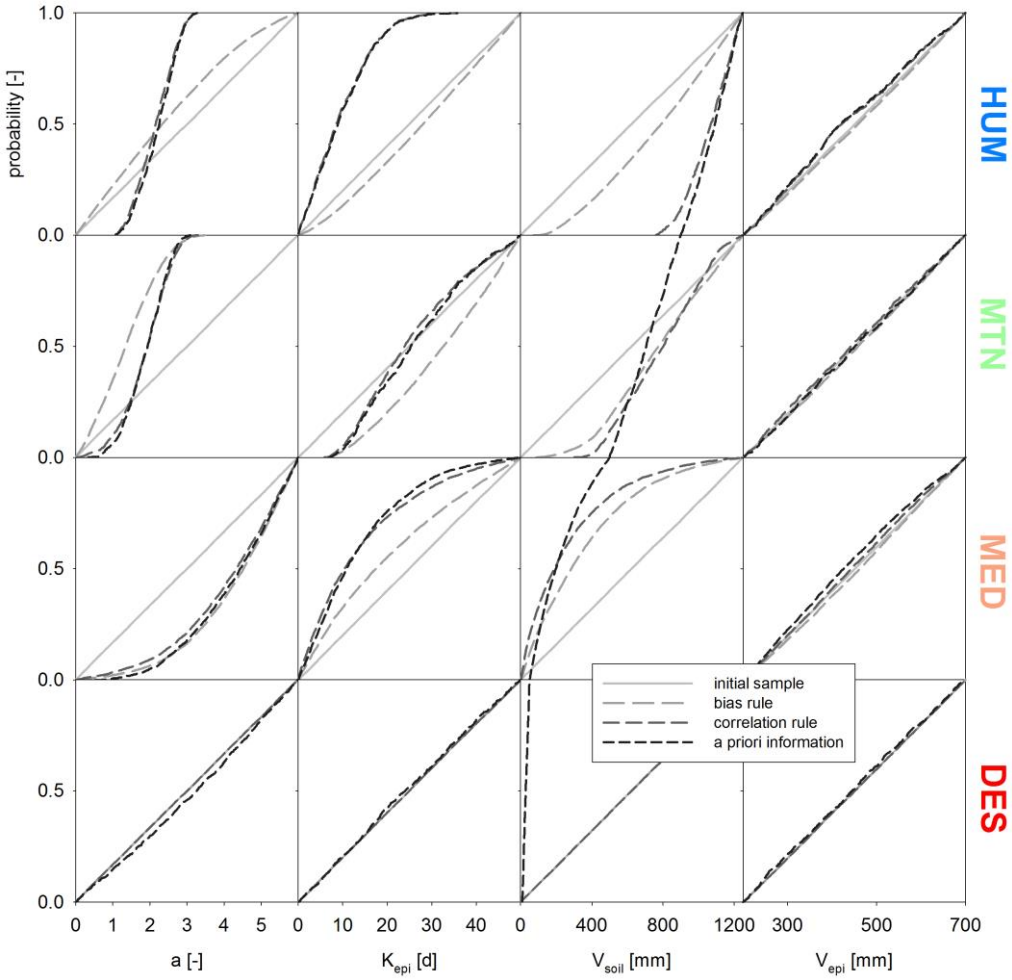

949

950 **Figure 6: Evolution of *posterior* probabilities of the 4 model parameters for the 4 karst landscapes along**
951 **the steps of the parameter confinement strategy.**

952

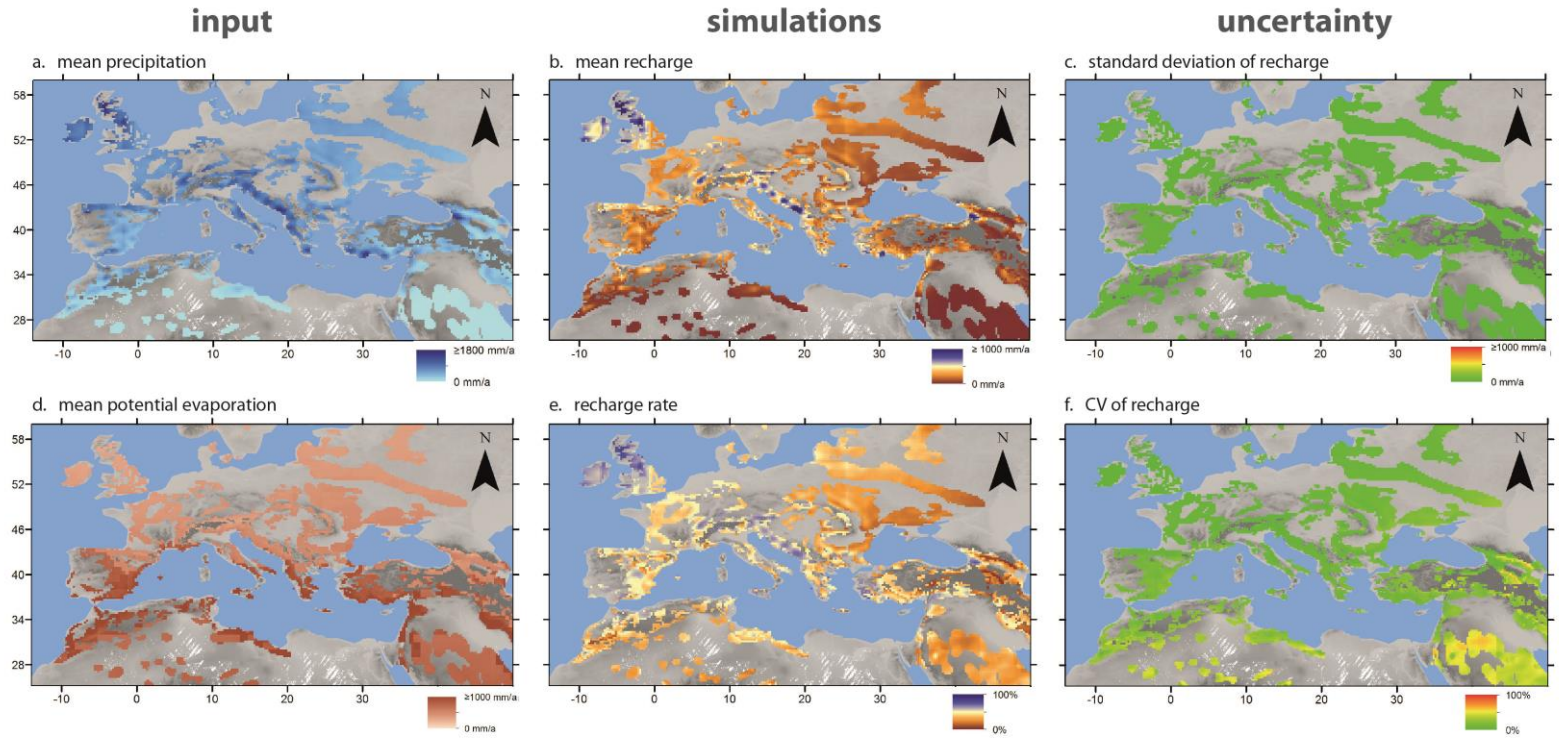

953

954 **Figure 7: (a) Observed precipitation and (d) potential evaporation versus the simulated (b) mean annual recharge and (e) mean annual recharge rates derived**
955 **from the mean of all 250 parameter sets, and (c) the standard deviation and (f) coefficients of variation of the simulations due to the variability among the 250**
956 **parameter sets.**

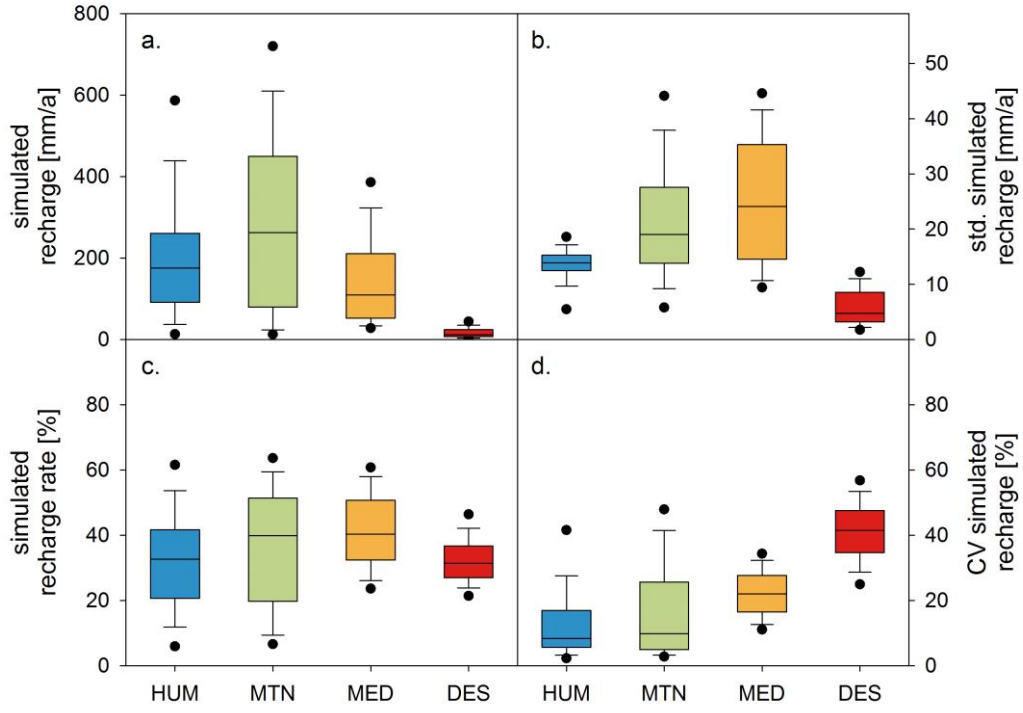

957

958 **Figure 8: (a) Simulated mean annual recharge, among the 4 karst landscapes, (b) their standard**
959 **deviations, (c) recharge rates, and (d) coefficients of variation obtained by the final sample of parameters.**

960

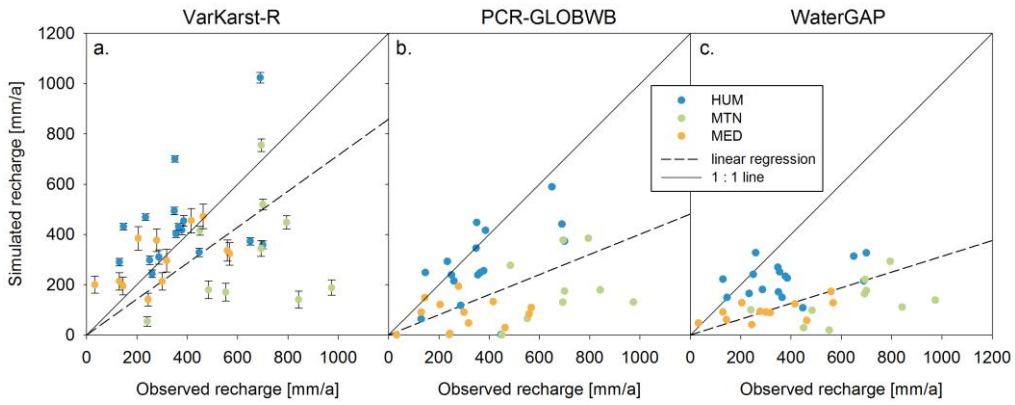

961

962 **Figure 9: Observations of mean annual recharge from independent studies (Table 3) versus the simulated**
963 **mean annual recharge by the VarKarst-R and the PCR-GLOBWB model (no data for the DES region**
964 **available)**

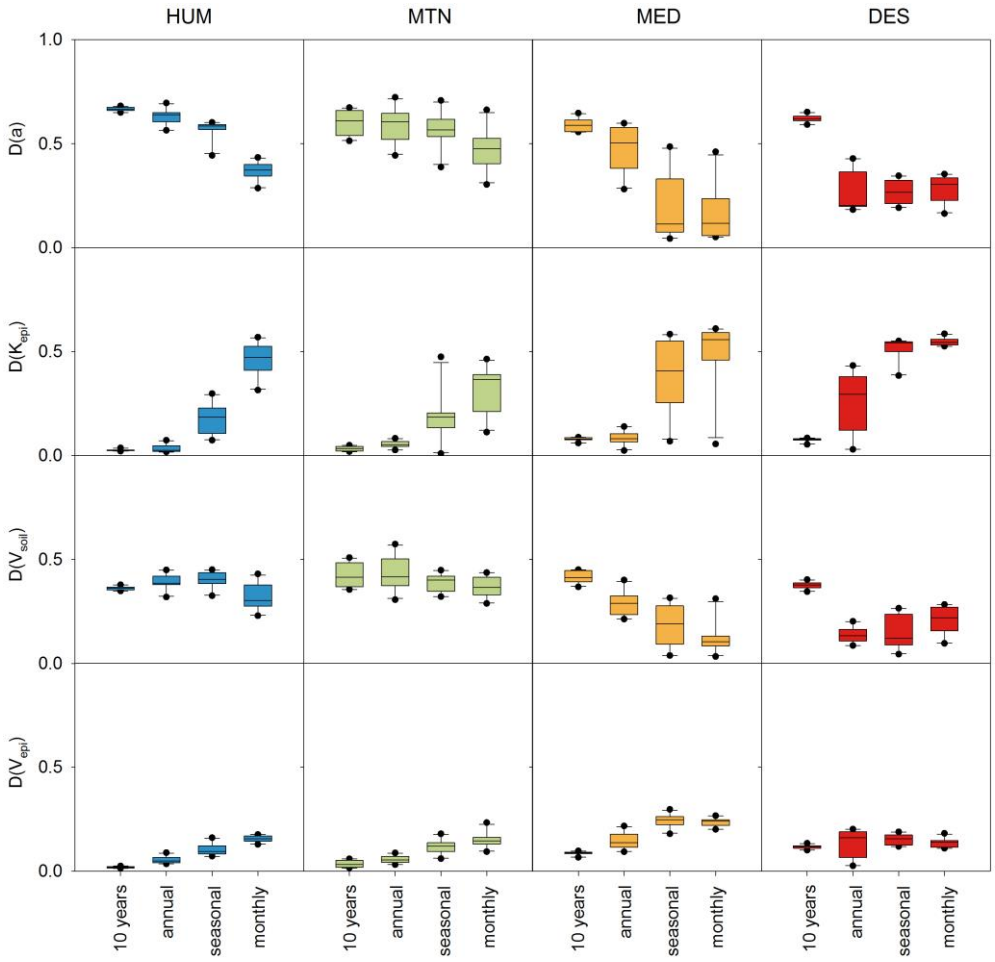

Figure 10: Sensitivity of simulated recharge to the model parameters at different time scales and in the different karst landscapes. Sensitivity is measured by the maximum distance (D) between the distribution of parameter sets that produce 'low' recharge (i.e. below the median) and the distribution producing 'high' recharge (above the median). Parameter sets are initially sampled from the ranges in Table 2.

6 Appendix

6.1 Results of the cluster analysis

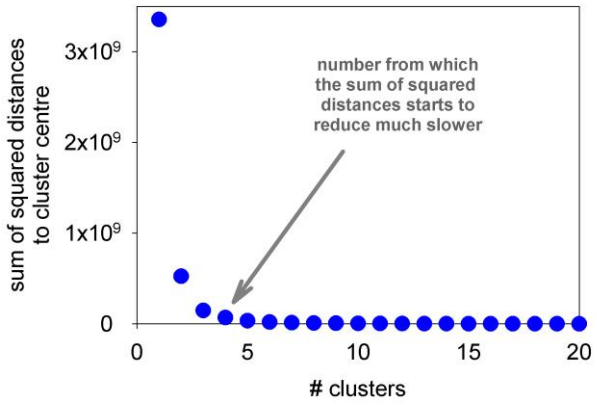

Figure A 1: Elbow plot of sum of squared distances to cluster centres for k-means method

6.2 Results of the regional sensitivity using initial ranges

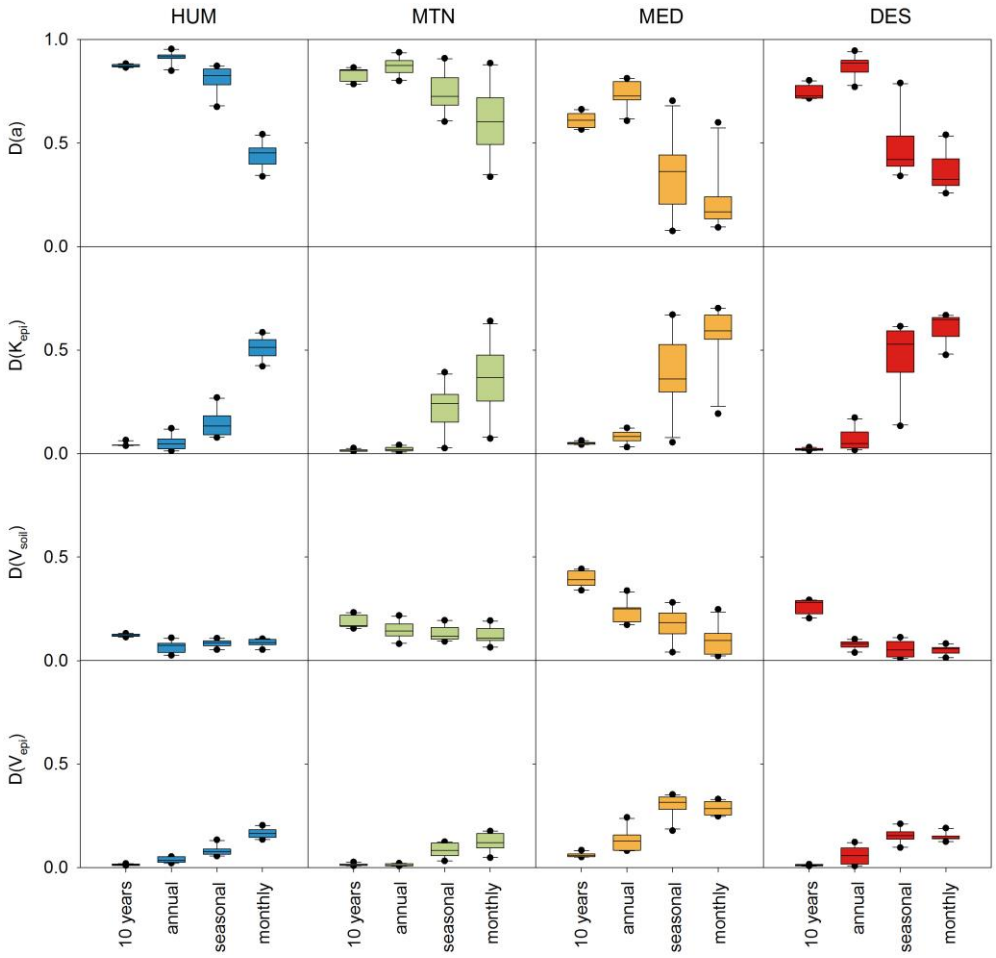

Figure A 2: Sensitivity of simulated recharge to the model parameters at different time scales and in the different karst landscapes, as in Figure 10 but sampling parameters from the confined parameter ranges of Table 5~~Table 5~~